Physics of Fluids

Large eddy simulations of turbulent planar jets of viscoelastic fluids

Cite as: Phys. Fluids **33**, 045110 (2021); https://doi.org/10.1063/5.0039826
Submitted: 07 December 2020 . Accepted: 15 February 2021 . Published Online: 07 April 2021

S. Parvar, C. B. da Silva, and F. T. Pinho

Physics of Fluids ARTICLE scitation.org/journal/phf

Large eddy simulations of turbulent planar jets of viscoelastic fluids

Cite as: Phys. Fluids **33**, 045110 (2021); doi: 10.1063/5.0039826
Submitted: 7 December 2020 · Accepted: 15 February 2021 ·
Published Online: 7 April 2021

View Online Export Citation CrossMark

S. Parvar,[1,2] C. B. da Silva,[3] and F. T. Pinho[1,a)]

AFFILIATIONS

[1]CEFT/FEUP, Universidade do Porto, Rua Dr. Roberto Frias, 4200-465 Porto, Portugal
[2]INEGI, Campus da FEUP, Rua Dr. Roberto Frias, 4200-465 Porto, Portugal
[3]LAETA, IDMEC, Instituto Superior Técnico, Universidade de Lisboa, Lisboa, Portugal

[a)]**Author to whom correspondence should be addressed:** fpinho@fe.up.pt

ABSTRACT

Direct numerical simulations and large-eddy simulations of turbulent planar jets are used to assess the distortion similarity (DSIM) model, recently developed by Ferreira *et al.* ["Large-eddy simulations of forced isotropic turbulence with viscoelastic fluids described by the finitely extensible nonlinear elastic rheological model with Peterlin's closure model," Phys. Fluids **28**, 125104 (2016)] for homogeneous turbulence, in the simulation of turbulent viscoelastic planar jets. Both *a priori* and *a posteriori* tests of the DSIM model are used and show that the several assumptions used in the development of the DSIM model hold well in inhomogeneous free turbulent viscoelastic flows, e.g., (i) the scale similarity of the subgrid-scale (SGS) polymer stretching and (ii) the local equilibrium of the elastic energy production and dissipation. The DSIM model for the SGS polymer stretching term, together with the dynamic Smagorinsky model, is able to reproduce well the flow structures and the classical one-point statistics of turbulent viscoelastic planar jets. The model should be equally able to simulate other free shear flows of viscoelastic fluids, e.g., wakes and mixing layers.

NOMENCLATURE

A_{U_c}	The slope of the law of variation of centerline velocity (−)
A_δ	The slope of the law of variation of the jet width (−)
A_{τ_c}	The slope of the laws of variation of centerline stress (−)
C_{Dyn}	Coefficient of dynamic Smagorinsky model (−)
C_{ij}	Conformation tensor (−)
C_{sm}	Coefficient of classical Smagorinsky model (−)
$E(\kappa)$	Energy spectrum ($m^2\ s^2$)
$f(C_{kk})$	Peterlin function (−)
H	Width of the inlet slot (m)
L	Dumbbell maximum extensibility (−)
L_x, L_y, L_z	Computational domain length in the x, y, z directions (m)
n_x, n_y, n_z	Number of grid points in the x, y, z directions
P	Pressure (Pa)
Re	Reynolds number (−)
S_{ij}	Strain rate tensor (s^{-1})
$\lvert S\rvert$	Norm of the strain rate tensor (s^{-1})
T	Time (s)
u,v,w	Velocity in streamwise, normal, and spanwise direction (ms^{-1})
u_i	Velocity vector (ms^{-1})
U_J	Peak velocity at the inlet (ms^{-1})
U_∞^{in}	Co-flow velocity (ms^{-1})
x_i	i-th space coordinate (m)
X'	Fluctuation of X
$\overline{X}$	X low pass filtered in space
$\langle X\rangle_a$	Spatial averaging of X along a-direction

Greek letter

β	Ratio of kinematic viscosities (−)
δ_{ij}	Kronecker delta
δ_u	Mean flow thickness of the planar jet (m)
Δ	Filter size (m)
Δt	Time step (m)
$\Delta x, \Delta y, \Delta z$	Grid spacing in the x, y, z directions (m)
ε_s	Turbulent kinetic energy dissipation ($m^2\ s^{-3}$)
η	Kolmogorov length micro-scale (m)

κ Wave number (m^{-1})
λ Relaxation time of polymer (s)
υ_p Polymer kinematic viscosity ($m^2\ s^{-1}$)
υ_s Solvent kinematic viscosity ($m^2\ s^{-1}$)
υ_t Turbulent kinematic viscosity ($m^2\ s^{-1}$)
ρ Fluid density ($kg\ m^{-3}$)
τ_{ij}^{P} Polymer stress tensor (Pa)
τ_{ij}^{R} Residual stress tensor (Pa)
τ_{ij}^{S} Solvent stress tensor (Pa)
ψ_{ij} SGS polymer convection tensor (s^{-1})
ω Vorticity vector (s^{-1})

Subscripts and superscripts

[s] Refers to solvent
[p] Refers to polymer

I. INTRODUCTION

In 1949, Toms[1] found that adding a small number of polymeric molecules into Newtonian fluids induces severe drag reduction (DR), of up to 80% in turbulent pipe flow, which also naturally leads to a concomitant reduction in heat transfer. Industrial settings where viscoelastic fluids flow under turbulent conditions and lead to DR are oil transport in pipelines and well drilling for the oil and gas industries.[2] Other proposals have been put forward to use viscoelastic fluids in order to benefit from turbulent drag and heat transfer reductions such as in district heating and cooling systems,[3] firefighting equipment, and sewage systems. Operation in these two last applications are under extreme conditions: in firefighting, the aim is to increase the length of the jet, whereas the increase in flow rate at constant head due to drag reduction is very useful to increase the capacity of sewage systems during floods.[4] Other fields of application include the design of ships and submarines since drag reduction leads to more efficient energy use,[5] increasing the mixing rates in microfluidic applications[6] and biofluid systems.[7,8] Reducing the energy consumption rate in irrigation systems and in percolation through the soil is another motivation to use this phenomenon.[9] Some applications of drag reduction with viscoelastic fluids are also encountered in medicine during surgery when some blood analogs are used.[10,11] Hence, it comes as no surprise the wealth of research on this topic as reviewed in detail by Lumley,[12] Virk[13] and more recently White and Mungal.[14]

Direct numerical simulation (DNS) is the most accurate existing numerical technique to simulate turbulent flows. However, it requires very fine computational grids, with the number of grid points on the order of $O(Re^{9/4})$, and very small time steps in order to capture all the multiscale features of turbulent motion,[15,16] in addition to large memory requirements. For these reasons, DNS is not suited for fast engineering calculations and is still restricted to simple flows at moderate Reynolds numbers for assisting our understanding of the flow physics and the development of turbulence models for engineering computations.[17] This is particularly true when one considers DNS of turbulent flows of viscoelastic fluids since the computational cost of these simulations is substantially higher than for DNS of Newtonian fluids due to the additional rheological variables and corresponding governing equations and the numerical limitations imposed by fluid viscoelasticity.

Currently, the numerical simulation of engineering flows under turbulent flow conditions relies on the use of the Reynolds-averaged Navier–Stokes equations (RANS) proposed by Reynolds[18] due to the low or reasonable computational cost. RANS is based on the Reynolds decomposition of the physical variables and subsequent averaging of the governing equations, which introduces new unknowns that need to be modeled. There are some available RANS models for turbulent flows of viscoelastic fluids,[19–23] which were developed based on wall turbulent flows. However, RANS has well known limitations when dealing with unsteady and transient flows, flows with separation, and rotation and flows faced with strong curvatures. Moreover, although RANS models may be able to predict the mean properties of many flows, some important flow characteristics cannot be estimated, such as the dominating flow frequencies. Large eddy simulation (LES) is a numerical technique that is usually suggested as the best candidate to handle the limitations of RANS without incurring in the massive cost of DNS. LES can be seen as an intermediate approach between DNS and RANS, which was initially developed to simulate atmospheric flows[24] and that was latter used to simulate wall bounded flows.[25] In LES, the large scales of motion (or resolved or grid-scales, GS) are explicitly simulated, while the effects of the small scales of motion, or subgrid-scales (SGS), are modeled. The SGS term arises when low-pass filtering the Navier–Stokes equations and needs to be modeled. A comprehensive review of LES approaches can be found in Refs. 26–28.

The main role of any SGS model consists in assuring the correct amount of kinetic energy transfer between the resolved and unresolved scales, and is consequently heavily derived from the classical Richardson–Kolmogorov energy cascade concept.[15,29] When the turbulence arises in a non-Newtonian fluid, the energy cascade mechanism becomes considerably more complicated due to the interaction of the velocity fluctuations with the fluid rheology variables across a large range of space and time scales. Indeed, non-Newtonian fluids are characterized by a variety of rheological constitutive equations.[30,31] There are ongoing debates regarding what are the appropriate constitutive equations needed to describe dilute polymer solutions.[32,33] However, one of the simplest constitutive equations used is the finitely extensible nonlinear elastic rheological model with Peterlin's closure (FENE-P), which is able to describe the main features of the rheology of dilute polymer solutions,[30,31,34–36] such as memory effects, shear-thinning, and bounded elastic stresses. For these reasons, the FENE-P model has been used in many studies of turbulent viscoelastic fluid flows.[37–40]

The interaction between the solvent and the polymer molecules greatly complicates the kinetic energy cascade, particularly in the so-called inertio-elastic turbulence, which occurs when the polymer relaxation times are larger than the Kolmogorov time scale.[37,40] For instance, it was observed that in this regime the polymer additives dissipate the main portion of the kinetic energy transferred from the large to the small scales of motion, which may lead to the establishment of a second, polymer induced, kinetic energy cascade.[37–40] This polymer-induced energy cascade competes with the classical (nonlinear) energy cascade[39–41] and therefore greatly complicates the GS/SGS interactions that play a vital role in the dynamics of turbulent flows and that need to be understood and modeled into the SGS terms aiming to simulate turbulence in viscoelastic fluids. Note in this respect that low-pass filtering the rheological constitutive equation for viscoelastic fluids also gives rise to new SGS terms there.

There are only a few studies about the SGS model in the momentum equation for turbulent flows of non-Newtonian fluids. Ohta and

Miyashita[42] extended the Smagorinsky model, by considering the effect of variable viscosity, to study turbulent channel flow of various types of purely viscous non-Newtonian fluids based on power laws. Thais *et al.*[43] proposed the first SGS model for temporal large eddy simulations (TLES) of viscoelastic fluid flows based on the FENE-P constitutive equation. Their SGS model was based on a temporal approximate deconvolution method (TADM) for both the SGS terms of the solvent and polymer stresses in momentum and conformation tensor equations. Although the TLES model has good accuracy in DR predictions, at least when using fine meshes, it is highly complex because of the deconvolution procedures involved, and for this reason, it is likely to demand considerable computational cost. Moreover, the model is entirely based on mathematical procedures, without any physical input from the interaction between the turbulent fluctuations and the fluid elasticity. Wang *et al.*[44] used the TLES model in forced homogeneous isotropic turbulence (FHIT) of FENE-P fluids at moderate Taylor scale Reynolds number and verified the results with the corresponding DNS results. Li *et al.*[45] investigated the DR in viscoelastic turbulent channel flows using the TLES model[43] by filtering their constitutive equation, a simplified version of a multi-mode FENE-P model.

Masoudian *et al.*[46] carried out *a priori* tests in order to analyze and evaluate the effect of the polymer additives on the SGS energy in the filtered momentum and FENE-P constitutive equations in turbulent channel flow of viscoelastic fluids. They were able to identify which terms become negligible and which require modeling when the filtering operation was applied to the FENE-P evolution equations. The subgrid-scale advection term in the filtered conformation tensor equation is an example of the former, whereas the subgrid-scale distortion in the same equation is an example of the latter.

To deal with the subgrid-scale distortion in the evolution equation for the conformation tensor in LES of forced isotropic turbulence of viscoelastic fluids, described by the FENE-P model, Ferreira *et al.*[37] proposed the distortion similarity model (DSIM). The SGS stresses arising in the solvent were modeled with the classical Smagorinsky model. The DSIM model relies on two main assumptions: (i) self-similarity of the polymer stretching term and (ii) global/local equilibrium of the trace of conformation tensor. The LES results from the DSIM model show that it predicts well many detailed quantities from forced isotropic turbulence of viscoelastic fluids, such as the solvent dissipation reduction (SDR), the shape of the kinetic energy spectra, and the shape and size of the coherent vortices. It is noteworthy that in contrast to previous models the DSIM model is simple to implement and exhibits a low computational cost.

The main motivation of the present work is to assess the DSIM model recently developed by Ferreira *et al.*[37] in inhomogeneous turbulent flow configurations. This model has been previously developed and assessed in isotropic turbulence, and it is important to test its performance in flows characterized by inhomogeneous conditions in order to isolate these conditions in the results obtained from the model. Although the ultimate goal of any newly developed subgrid-scale model must be to accurately simulate wall bounded flows, it is also well known that LES of wall bounded flows faces considerable challenges that have not much to do with the core of the subgrid-scale model,[15] and the analysis of new subgrid-scale models is often blurred when they are assessed initially in wall flows due to the restricted "activity" of the models near walls.

Consequently, in the present study, we assess the DSIM model in a planar turbulent jet flow since it provides a simple configuration to consider the effects of inhomogeneity, without facing the difficulties that arise in the presence of solid walls. Our study is inspired from Masoudian *et al.*[46] and uses the recently published DNS results from Guimarães *et al.*[47] to assess several modeling hypotheses. Then, the DSIM subgrid-scale model is implemented in our in-house DNS code and its performance is assessed through *a posteriori* tests.

The paper is organized as follows. Sections II and III discuss the flow problem and present the governing equations for flows of viscoelastic fluids described by FENE-P model and filtered governing equations, respectively. Section IV presents the main numerical techniques and algorithms used in the present study. Sections V and VI assess the model using *a priori* and *a posteriori* tests, respectively. The paper ends with an overview of the main conclusions.

II. FLOW PROBLEM AND GOVERNING EQUATIONS

A planar jet is a type of free shear layer flow in which a stream of high momentum is discharged into the same or another fluid at rest; in this work, the former situation is considered. Figure 1 shows the Cartesian coordinate system used in the present work, where the main flow direction (streamwise) is x, and the jet spreads in the normal direction (y), while the flow is homogeneous in the spanwise (z) direction. U_J is the uniform streamwise velocity at the inlet nozzle, U_∞^{in} is the jet co-flow velocity, and H is the inlet slot-width of the jet. According to the classical jet theory (for a Newtonian fluid), the turbulent planar jet flow in the far field is statistically two-dimensional and is independent of Reynolds number, provided the Reynolds number is high enough.[15]

The jet half-width is defined as the transverse distance between the centerline and the location where the mean streamwise velocity equals half the mean centerline velocity; however, in the present study, we use a different definition for the jet shear layer thickness $\delta(x)$, introduced by Guimarães *et al.*[47] It assumes that the volumetric flow rate remains constant and is equal to $\dot{V}(x) = 2L_z\delta(x)U_c(x)$, where $U_c(x)$ is the value of the mean velocity at the centerline and L_z is the computational domain length in the spanwise direction. Since the flow

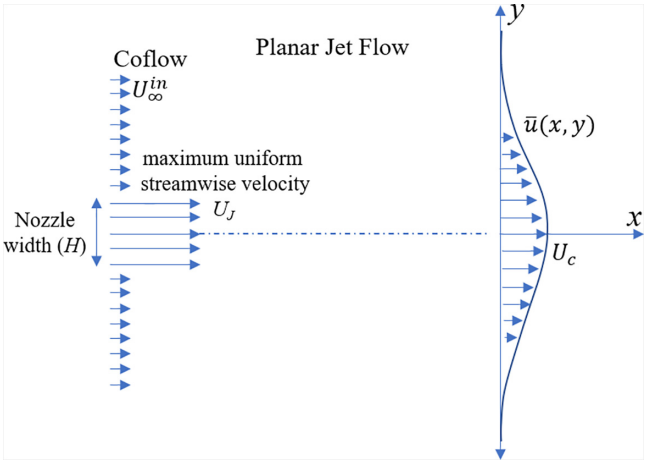

FIG. 1. The schematic of planar jet flow.

rate of the jet is obtained from $\dot{V}(x) = 2L_z \int_0^\infty \overline{u}(x,y)dy$, the jet shear thickness defined in Ref. 47 is

$$\delta(x) = \int_0^\infty \frac{\overline{u}(x,y)}{U_c(x)} dy, \tag{1}$$

where $\overline{u}(x,y)$ is the profile of mean streamwise velocity.

A. The governing equations of FENE-P fluids

The FENE-P model is used to describe the rheology of the dilute polymer solutions. In this model, the effects of an ensemble of molecules located at any given point are represented by dumbbells, each consisting of a pair of beads connected by a massless nonlinear spring.

The mass conservation and momentum equations for an incompressible isothermal flow are

$$\frac{\partial u_k}{\partial x_k} = 0, \tag{2}$$

$$\rho\left(\frac{\partial u_i}{\partial t} + u_k \frac{\partial u_i}{\partial x_k}\right) = -\frac{\partial P}{\partial x_i} + \frac{\partial \tau_{ij}}{\partial x_j}, \tag{3}$$

where u_i is the velocity vector, P is the pressure, ρ is the fluid density, and τ_{ij} is the total stress tensor which is calculated as the sum of a Newtonian solvent contribution (τ_{ij}^s) and a polymeric contribution (τ_{ij}^p)[19,20,30,31]

$$\tau_{ij} = \tau_{ij}^s + \tau_{ij}^p. \tag{4}$$

The solvent stress τ_{ij}^s is described by Newton's law of viscosity with solvent kinematic viscosity υ_s

$$\tau_{ij}^s = 2\rho\upsilon_s S_{ij}, \tag{5}$$

where S_{ij} is the rate-of-strain tensor, defined as

$$S_{ij} = \frac{1}{2}\left(\frac{\partial u_i}{\partial x_j} + \frac{\partial u_j}{\partial x_i}\right). \tag{6}$$

The polymeric stress (τ_{ij}^p) of the FENE-P model relies on the following explicit equation:[19,20,30,31]

$$\tau_{ij}^p = \frac{\rho\upsilon_p}{\lambda}\left[f(C_{kk})C_{ij} - f(L)\delta_{ij}\right], \tag{7}$$

where υ_p is the polymer zero shear rate kinematic viscosity and C_{ij} is the conformation tensor. The conformation tensor expresses the orientation and stretch of the set of polymer dumbbells at each point, which is defined as

$$C_{ij} = \frac{\langle r_i r_j\rangle}{\langle R^2\rangle_0}, \tag{8}$$

where r_i is the end-to-end projection in i-direction of the vector connecting the two beads of the dumbbell. The second order moment $\langle r_i r_j\rangle$ is normalized by the square of its equilibrium radius $\langle R^2\rangle_0$, where $< >$ represents an ensemble average over the configuration space of the dumbbells. The FENE-P model also depends on λ, which is the longest relaxation time of the polymer molecules and δ_{ij} is the identity tensor. The Peterlin function is expressed by

$$f(C_{kk}) = \frac{L^2 - 3}{L^2 - C_{kk}}, \tag{9}$$

and its value at equilibrium is $f(L) = 1$, where L is the maximum dumbbell extensibility and C_{kk} is the trace of the conformation tensor. The conformation tensor obeys the following hyperbolic differential equation:

$$\frac{\partial C_{ij}}{\partial t} + u_k \frac{\partial C_{ij}}{\partial x_k} = C_{jk}\frac{\partial u_i}{\partial x_k} + C_{ik}\frac{\partial u_j}{\partial x_k} - \frac{1}{\lambda}\left[f(C_{kk})C_{ij} - f(L)\delta_{ij}\right]. \tag{10}$$

The first term on the left-hand side (LHS) of Eq. (10) is the local time variation of the conformation tensor and the second term is the advection term, while the first two terms on the right-hand side (RHS) account for the stretching and distortion of the polymer molecules. The last term on RHS represents the storage of elastic energy in the polymer molecules.

The two kinematic viscosity coefficients define the solvent viscosity ratio $\beta_s = \frac{\upsilon_s}{\upsilon_s+\upsilon_p} = \frac{\upsilon_s}{\upsilon_0}$, where the zero-shear rate viscosity of the fluid (υ_0) is the sum of solvent and polymer kinematic viscosities $\upsilon_0 = \upsilon_s + \upsilon_p$. Since the FENE-P model is used to describe dilute polymer solutions, the value of β_s in this work is restricted to $0.8 \le \beta_s \le 1$.

The governing equations above are valid for DNS of a viscoelastic flow described by the FENE-P model. However, the governing equations required for LES involve several additional SGS terms as described in Sec. III.

III. FILTERED GOVERNING EQUATIONS

To obtain the governing equation for LES of the viscoelastic fluids described by the FENE-P model, one needs to filter the equations of Sec. II, as described in detail in Masoudian *et al.*[46] and in Ferreira *et al.*,[37] so that any flow variable $\varphi(\vec{x},t)$, is split into the sum of a resolved (grid-scale-GS) $\overline{\varphi}(\vec{x},t)$, and an unresolved (subgrid-scale-SGS), contribution

$$\varphi(\vec{x},t) = \overline{\varphi}(\vec{x},t) + \varphi'(\vec{x},t). \tag{11}$$

The GS contribution is defined by a spatial low pass filtering operation

$$\overline{\varphi}(\vec{x},t) = \int_\Omega \overline{\varphi}(\vec{x}',t) G_\Delta(\vec{x}-\vec{x}')d\vec{x}', \tag{12}$$

in which G_Δ is the convolution kernel that determines the filter type, and Δ is the filter width. In the present study, a classical top-hat (box) convolution filter is utilized to separate the resolved and unresolved scales of motion, which for a one-dimensional case reads as

$$G_\Delta(x) = \begin{cases} \frac{1}{\Delta} & \text{if } |x| \le \frac{\Delta}{2}. \\ 0 & \text{otherwise} \end{cases} \tag{13}$$

The box filter is local in the physical space and nonlocal in the spectral space, but the filtering operation is equivalent to a finite difference or finite volume discretization, which are commonly used in LES of engineering applications.[16] By applying the low pass filter to the governing equations, the filtered continuity and momentum equations are obtained (Masoudian *et al.*[46] and in Ferreira *et al.*[37])

$$\frac{\partial \overline{u}_k}{\partial x_k} = 0, \tag{14}$$

$$\frac{\partial \overline{u}_i}{\partial t} + \overline{u}_j \frac{\partial \overline{u}_i}{\partial x_j} = -\frac{1}{\rho}\frac{\partial \overline{P}}{\partial x_i} + \upsilon_s \frac{\partial}{\partial x_j}[2\overline{s}_{ij}] + \frac{\partial \overline{\tau_{ij}^{sgs}}}{\partial x_j} + \frac{\partial \overline{\tau_{ij}^{p}}}{\partial x_j}, \tag{15}$$

where $\overline{\tau_{ij}^{sgs}} = [\overline{u_i u_j} - \overline{u}_i \overline{u}_j]$ is the SGS tensor and the last term on the RHS of Eq. (15) is the filtered polymer stress contribution given by

$$\overline{\tau_{ij}^{p}} = \frac{\rho \upsilon_p}{\lambda}\left[\overline{f(C_{kk})C_{ij}} - f(L)\delta_{ij}\right]. \tag{16}$$

Equation (16) can be re-written as

$$\overline{\tau_{ij}^{p}} = \frac{\rho \upsilon_p}{\lambda}\left[f(\overline{C}_{kk})\overline{C}_{ij} + \chi_{ij} - f(L)\delta_{ij}\right]. \tag{17}$$

in which the SGS of the filtered $\overline{f(C_{kk})C_{ij}}$, is defined as

$$\chi_{ij} = \overline{f(C_{kk})C_{ij}} - f(\overline{C}_{kk})\overline{C}_{ij}. \tag{18}$$

The filtered evolution equation for the conformation tensor is

$$\frac{\partial \overline{C}_{ij}}{\partial t} + \overline{u_k \frac{\partial C_{ij}}{\partial x_k}} = \overline{\frac{\partial u_i}{\partial x_k} C_{jk}} + \overline{\frac{\partial u_j}{\partial x_k} C_{ik}} - \frac{1}{\lambda}\left[\overline{f(C_{kk})C_{ij}} - \delta_{ij}\right], \tag{19}$$

where the last term on the LHS is the filtered advection of the conformation tensor, and the first two terms on the RHS are the filtered polymer stretching, whereas the last term on the RHS is the filtered polymer dissipation. Equation (19) can be re-written in a way that singles out the resolved and subgrid-scale quantities in the conformation tensor equation as discussed previously,[37,46] namely,

$$\frac{\partial \overline{C}_{ij}}{\partial t} + \overline{u}_k \frac{\partial \overline{C}_{ij}}{\partial x_k} = \frac{\partial \overline{u}_i}{\partial x_k}\overline{C}_{jk} + \frac{\partial \overline{u}_j}{\partial x_k}\overline{C}_{ik} - \frac{1}{\lambda}\left[f(\overline{C}_{kk})\overline{C}_{ij} + \chi_{ij} - \delta_{ij}\right] - \psi_{ij} + \gamma_{ij}, \tag{20}$$

with χ_{ij} defined in Eq. (18), the unresolved (SGS) conformation advection tensor defined as

$$\psi_{ij} = \overline{u_k \frac{\partial C_{ij}}{\partial x_k}} - \overline{u}_k \frac{\partial \overline{C}_{ij}}{\partial x_k}, \tag{21}$$

and the SGS polymer stretching tensor given by

$$\gamma_{ij} = \left[\overline{\frac{\partial u_i}{\partial x_k} C_{jk}} - \frac{\partial \overline{u}_i}{\partial x_k}\overline{C}_{jk}\right] + \left[\overline{\frac{\partial u_j}{\partial x_k} C_{ik}} - \frac{\partial \overline{u}_j}{\partial x_k}\overline{C}_{ik}\right]. \tag{22}$$

Now, closures need to be developed for all SGS terms in all governing equations. In principle the SGS stress tensor in the momentum equation may be affected by fluid rheology. However, since this is the very first work developing models for LES of viscoelastic fluids in jets and $\overline{\tau_{ij}^{sgs}}$ quantifies inertial effects, as a first approximation we will consider that the closures developed for $\overline{\tau_{ij}^{sgs}}$ with Newtonian fluids remain valid and the effect of polymers on it is carried over through the filtered velocity and rate of deformation fields. The closures used for $\overline{\tau_{ij}^{sgs}}$ are presented next.

A. Smagorinsky model (Sm)

Solution of the LES equations requires closures for all the SGS terms. In the present work the SGS stress tensor $\overline{\tau_{ij}^{sgs}}$ is modeled using two different closures: the classical and the dynamic Smagorinsky models. Both models were previously implemented in the present planar jet flow code (for Newtonian fluids) by Silva *et al.*[48,49]

The Smagorinsky model was originally developed by Smagorinsky[24] and is based on an eddy viscosity given by

$$\nu_t(x,t) = \left(C_{Sm}\overline{\Delta}\right)^2 |\overline{S}|, \tag{23}$$

where $|\overline{S}| = \left(2\overline{S}_{ij}\overline{S}_{ij}\right)^{1/2}$ is the filtered strain rate magnitude, and $\overline{S_{ij}}$ is the filtered rate-of-strain which is obtained by filtering Eq. (6), C_{Sm} is the Smagorinsky constant,, and $\overline{\Delta}$ is the filter size calculated by $\overline{\Delta} = (\Delta x \times \Delta y \times \Delta z)^{\frac{1}{3}}$.[16] The main drawback of the classical Smagorinsky model is that it cannot consider backward energy transfer since it is a dissipative closure: the local equilibrium assumption is not valid and the model is too dissipative. However, the Smagorinsky model is simple, with a very low computational cost, therefore, it is popular in the study of turbulent flows. In the present work, we take $C_{Sm} = 0.16$ for the Smagorinsky constant.[48,49] This model, with the same value of C_{Sm}, was used previously by Ferreira *et al.*[37] for FENE-P fluids in forced homogeneous isotropic turbulence, with very good results.

B. Dynamic Smagorinsky model (Dyn)

To deal with the limitations of the classical Smagorinsky closure, the dynamic Smagorinsky model was proposed by Germano *et al.*[50] Here, the eddy viscosity is still given by Eq. (23), but with C_{Dyn} instead of C_{Sm}, where C_{Dyn} is assumed to depend on time and space and computed by utilizing the Germano identity. As a result, the coefficient is now computed in the entire domain as $C_{Dyn}(x,y,t) = \frac{\langle M_{ij}L_{ij}\rangle}{\langle M_{pq}M_{pq}\rangle}$, where $\langle\rangle$ represents an averaging in the homogenous flow direction, which in the present planar jet flow is the z-direction. The coefficient depends on the Leonard stress tensor

$$L_{ij} = \widetilde{\overline{u}_i\overline{u}_j} - \widetilde{\overline{u}}_i\widetilde{\overline{u}}_j, \tag{24}$$

obtained by applying a spatial test filter, of size equal to 2 Δ and identified by the tilde, and on

$$M_{ij} = (k\Delta)^2 |\widetilde{\overline{S}}|\widetilde{\overline{S}}_{ij} - \Delta^2 \widetilde{|\overline{S}|\overline{S}_{ij}}. \tag{25}$$

For a test filter size equal to 2Δ, the coefficient k is assumed to be $k = \sqrt{5}$, $|\overline{S}|$ is defined in Sec. III A and $|\widetilde{\overline{S}}| = \sqrt{2\widetilde{\overline{S}}_{ij}\widetilde{\overline{S}}_{ij}}$ is the magnitude of the double filter sized of the large-scale strain rate tensor. To prevent the existence of numerical instabilities during the simulations, due to excessively large negative values of coefficient C_{Dyn}, a clipping procedure was implemented and $C_{Dyn} \geq 0$ was imposed everywhere.

IV. NUMERICAL METHODS

The in-house code used to solve the original governing equations through DNS and the filtered governing equation (LES) is the same. Recently, our in-house DNS solver has been extended by Guimarães *et al.*[47] to simulate turbulent flows of FENE-P fluids. The code was originally developed by Reis[51] and later by Lopes[48] who added some LES closures[48,49] for Newtonian fluids. The code uses a sixth-order compact differencing scheme[52] in the streamwise (x) direction and a pseudo-spectral method[53] in the normal (y) and spanwise (z) directions.[29] An explicit three-step third-order low-storage Runge–Kutta

time-stepping scheme is used for temporal discretization. For the present studies, the new closures associated with the constitutive equations, to be discussed below, were added to the code.

Discontinuities in the polymer stresses are the main difficulty in implementing the FENE-P model because of the growth of Hadamard instabilities.[55] Several methods have been proposed by utilizing artificial stress diffusivity or the slope limiter to handle this problem such as in Refs. 55–59. Although they can prevent the Hadamard instabilities, they may affect the computation of the polymer stresses or produce negative eigenvalues in the conformation tensor, leading to errors in the conservation laws.[57–60] In 2006, Vaithianathan *et al.*[60] utilized the Kurganov and Tadmor (or KT)[61] numerical scheme to handle all mentioned issues. The KT scheme is a central difference, second-order accurate in physical space, and independent of the time step. The KT scheme assures that the conservation laws for conformation tensor are satisfied. Details of this procedure in the present code are described in detail in Refs. 47, 61, and 62. The implementation of the KT scheme in the present code was carried out by Guimarães *et al.*[47] and the semi-analytical solution for the laminar planar jet flow of FENE-P fluids of Parvar *et al.*[63,64] was also used to verify the implementation.

V. *A PRIORI* TESTS: DNS OF TURBULENT PLANAR JET FENE-P FLUID

To develop closures for the remaining SGS terms appearing in the constitutive equation, we perform *a priori* tests by using the DNS data of turbulent viscoelastic planar jet flows of Guimarães *et al.*[47] The physical and computational characteristics of these simulations are now described, with more details given in Guimarães *et al.*[47]

A hyperbolic tangent profile is used as an inlet condition for the mean inlet velocity profile,[29]

$$\overline{u}(x=0,y)=\frac{U_J+U_\infty^{\text{in}}}{2}+\frac{U_J-U_\infty^{\text{in}}}{2}\tanh\left[\frac{H}{4\theta}\left(1-\frac{2|y|}{H}\right)\right], \quad (26)$$

where U_J is the maximum mean streamwise velocity and U_∞^{in} is the jet co-flow velocity. For the conformation tensor profiles at the inlet, conditions of fully-developed channel flow were assumed with the shear rate computed from the velocity profile of Eq. (26), as given by Pinho *et al.*.[19] Periodic boundary conditions are used for the lateral boundaries (y and z directions). In addition, the amplitude of noise for all inlet velocity fluctuations of DNS is set at 10%, and the ratio between the inlet slot-width and the momentum thickness is $H/\theta = 30$.[47,49] The Reynolds number (Re) is defined by

$$Re_H=\frac{(U_J-U_\infty^{\text{in}})H}{\upsilon_s}, \quad (27)$$

where H is the inlet slot-width of the jet and υ_s is the kinematic solvent viscosity. A global Weissenberg number is also defined as the ratio between the elastic and integral time scales, which for the turbulent jet is given by

$$Wi=\frac{\lambda(U_J-U_\infty^{\text{in}})}{H}. \quad (28)$$

In all simulations the Reynolds number was equal to $Re = 3500$, and the ratio between the solvent and the total viscosities (β_s) was set to $\beta_s = 0.8$. The computational domain length was equal to $18H$ and the grid size was $512 \times 512 \times 128$ in the streamwise, normal, and spanwise directions, respectively. The maximum extensibility of the dumbbell was set to $L^2 = 10^4$, while the relaxation time for the FENE-P fluid flows were $\lambda = 0.4$, 0.8 and 1.2 s, leading to the global Weissenberg numbers of $Wi = 1.1$, 2.2, and 3.3, respectively. A reference Newtonian DNS was also carried out for comparison and its results are indicated by subscript N. The main physical and computational details of the DNS are summarized in Table I (data extracted from Guimarães *et al.*[47]).

The statistical data extracted from the DNS of Guimarães *et al.*[47] was initially used to analyze the order of magnitude of each term in Eqs. (20)–(22), in order to simplify those equations by proposing relevant hypothesis, named (H1)–(H6) and finally to introduce the set of LES closures. It is important to mention that *a priori* tests were performed on the available instantaneous DNS data provided by Guimarães *et al.*,[47] but since the number of continuous instants of time provided was not very large, if we consider data at a specific x, y location the sample size is limited, even if data are averaged in the homogeneous direction (z), which we always do. Therefore, in order to increase the sample size we decided to perform the tests for the assessment of all hypotheses using the combination of all instantaneous data at the jet centerline ($y/H = 0$) inside the self-similar region ($10 \le x/H \le 18$). It is such large set of data that is used in Figs. 2–10, except for Fig. 3 where plotted data pertain to specific x, y values shown separately.

We are looking for closures for tensor-based quantities appearing in Eqs. (20)–(22) and these will necessarily involve coefficients which can be independent of the component (isotropic) or not (anisotropic). Both types of coefficient will be investigated here through the *a priori* testing, but when analyzing the isotropic coefficients we will rely on a governing equation for the filtered trace of the conformation tensor, as was done previously by Ferreira *et al.*[37] for forced homogeneous isotropic turbulence (FHIT). Additionally, for conciseness, when analyzing some SGS terms we will also show plots involving the corresponding quantities from the filtered trace equation. The equation for the evolution of the filtered trace of the conformation tensor can be written as

$$\underbrace{\frac{\partial \overline{C}_{ii}}{\partial t}}_{C_t}+\underbrace{\overline{u}_k\frac{\partial \overline{C}_{ii}}{\partial x_k}}_{C_a}=\underbrace{2\frac{\partial \overline{u}_i}{\partial x_k}\overline{C}_{ik}}_{C_p}-\frac{1}{\lambda}\left[\underbrace{f(\overline{C}_{kk})\overline{C}_{ii}+\chi_{ii}}_{C_d}-\delta_{ii}\right]-\psi_{ii}+\gamma_{ii}, \quad (29)$$

where C_t and C_a are the temporal and advection terms while C_p and C_d are the production and dissipation of the trace of the filtered conformation tensor components ($\overline{C}_{ii}$), respectively. The two remaining terms on the RHS of Eq. (29), ψ_{ii} and γ_{ii}, are the unknown subgrid-

TABLE I. Summary of physical and computational parameters of the DNS used to perform *a priori* tests, extracted from Guimarães *et al.*[47]. A_δ, A_{U_c}, and A_{τ_c} are slopes of the laws of variation of jet width (δ), mean centerline velocity (U_c), and centerline stress (τ_c) discussed later, domain size $\frac{L_x\times L_y\times L_z}{H^3} = 18 \times 18 \times 4.5$.

	Wi	λ (s)	β_s	L	Grid points	A_δ	A_{U_c}	A_{τ_c}
DNS_N	0	0	1.0	NA	$512 \times 512 \times 128$	0.110	0.21	NA
$DNS_{1.1}$	1.1	0.4	0.8	100	$512 \times 512 \times 128$	0.111	0.208	1.40
$DNS_{2.2}$	2.2	0.8	0.8	100	$512 \times 512 \times 128$	0.095	0.176	0.56
$DNS_{3.3}$	3.3	1.2	0.8	100	$512 \times 512 \times 128$	0.080	0.141	0.37

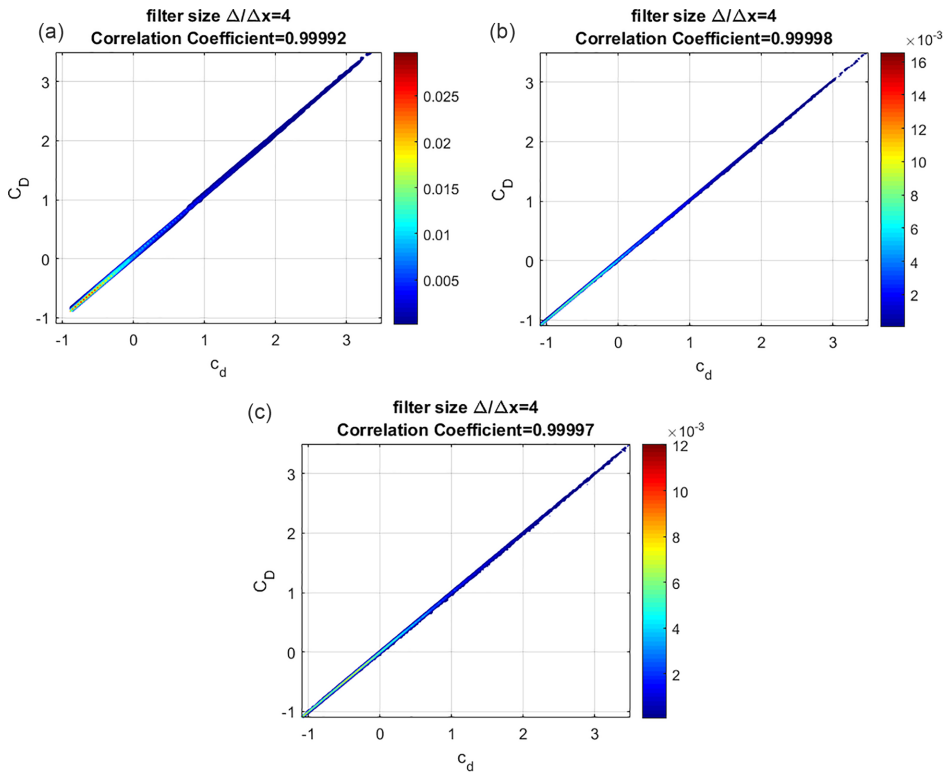

FIG. 2. Joint Probability density function (JPDF) of $c_d = \overline{f(C_{kk})C_{ii}}$ and $C_D = f(C_{kk})\overline{C_{ii}}$ normalized by their root mean square obtained from DNS at (a) $Wi = 1.1$, (b) 2.2, and (c) 3.3 with a filter size $\Delta/\Delta x = 4$. All data are from the jet centerline ($y/H = 0$) in the range $10 \leq x/H \leq 18$.

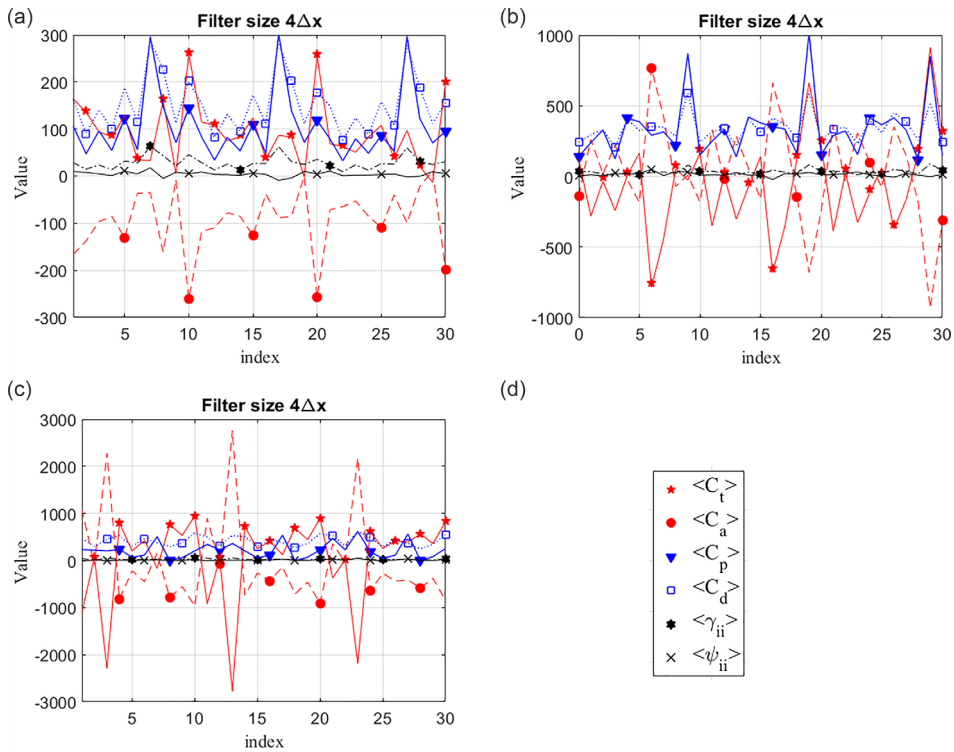

FIG. 3. The variation of terms in Eq. (29), averaged in the homogeneous direction, at a number of points (30) on the jet centerline ($y/H = 0$) for $10 \leq x/H \leq 18$. The DNS data pertain to (a) $Wi = 1.1$, (b) 2.2, and (c) 3.3. The legend is shown as part (d) and the filter size was $\Delta/\Delta x = 4$. Lines are a guide to the eye.

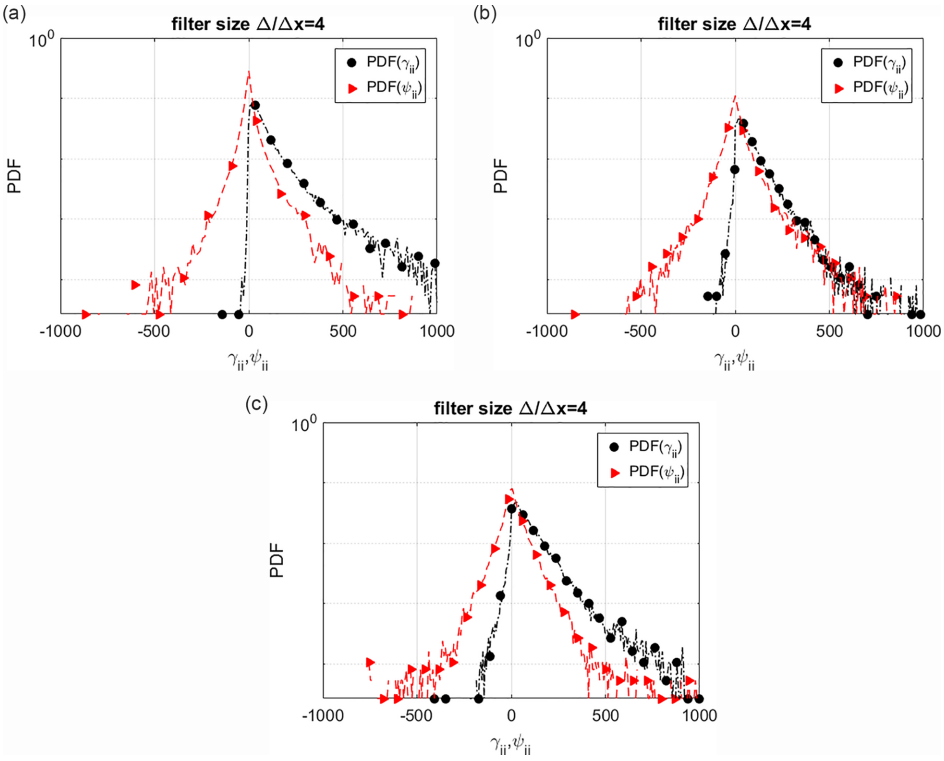

FIG. 4. PDF of the SGS of both advection of the trace of the conformation tensor and polymer stretching terms, obtained from DNS at (a) $Wi = 1.1$, (b) 2.2, and (c) 3.3 with a filter size $\Delta/\Delta x = 4$. All data are from the jet centerline ($y/H = 0$) in the range $10 \leq x/H \leq 18$. Lines are a guide to the eye.

scale contributions from the advection and polymer stretching, respectively, and χ_{ii} represents the SGS contribution to the dissipation of elastic energy.

Next, a series of six hypothesis will be tested in order to develop the closures needed by the filtered governing constitutive equation.

A. SGS of polymer dissipation: Hypothesis H1

The first hypothesis (**H1**) deals with the filtered nonlinear conformation tensor term (χ_{ij}) in the filtered conformation tensor evolution equation and in Eqs. (16)–(18) for the filtered polymer stress, which needs to be assessed in order to develop a LES closure.[36,45] The term can be decomposed as on the left side of the arrow in Eq. (30), where the difference inside the parentheses is the SGS contribution. The hypothesis is that the SGS term is very small and can be neglected; therefore, the filtered term equals the GS contribution as on the right-hand-side of the arrow in the following:

$$\overline{f(C_{kk})C_{ij}} = f(\overline{C}_{kk})\overline{C}_{ij} + \left(\underbrace{\overline{f(C_{kk})C_{ij}} - f(\overline{C}_{kk})\overline{C}_{ij}}_{\chi_{ij}}\right)$$
$$\rightarrow \overline{f(C_{kk})C_{ij}} \approx f(\overline{C}_{kk})\overline{C}_{ij} \text{ or } \chi_{ij} \cong 0. \quad (30)$$

Note that in homogeneous flows and considering the filtering properties for a box filter, one concludes that $\overline{f(C_{kk})} = f(\overline{C}_{kk})$. Even though the jet flow is not homogeneous, this equality will still be assumed.

Figures 2(a)–2(c) show the joint probability density function (JPDF) of the $c_d = \overline{f(C_{kk})C_{ii}}$ and $C_D = \overline{f(C_{kk})C_{ii}}$ in the viscoelastic turbulent planar jet flow for $Wi = 1.1$, 2.2, 3.3 and for a filter size equal to $\Delta/\Delta x = 4$(for filter sizes $\Delta/\Delta x = 2$ and 8 similar results are observed). The two quantities are strongly correlated, and the correlation coefficient is very close to 1, which means that the two quantities are closely matched. Note that the JPDF plotted involves the trace of the conformation tensor (C_{ii}), but hypothesis (**H1**) remains valid if the sink terms are assessed individually. These are not shown for conciseness. Masoudian *et al.*[46] and Ferreira *et al.*[37] reached similar results for turbulent channel flow and forced isotropic turbulence of FENE-P fluids, respectively. The results in Fig. 2 confirm the validity of assumption **H1** for a free flow in the presence of mean shear. Therefore, this assumption is used henceforth in the present study.

B. SGS of advection: Hypothesis H2

The second hypothesis **(H2)** deals with the subgrid-scale advection and we analyze next the corresponding term for the trace of the filtered conformation tensor, denoted ψ_{ii}, and defined according to Eq. (21).

Hypothesis **H2** assumes that the SGS contribution of the advection from the filtered conformation tensor equation is negligible when compared with the resolved advection term. Figures 3(a)–3(c) plot the variations of all terms of Eq. (29) averaged in the homogeneous direction; as shown $\langle\psi_{ii}\rangle$ is much smaller than the other quantities and, in particular, smaller than $\langle C_a\rangle$. In Fig. 3, we consider data at an instant of time at specific (x, y) points on the jet centerline, but within the self-similarity region. Each data point marked in the abscissa actually corresponds to the average of the 128 points in the homogeneous z-direction of the domain (at that value of (x, y)), i.e., in contrast to the figures showing the joint PDFs, we are not mixing data at all

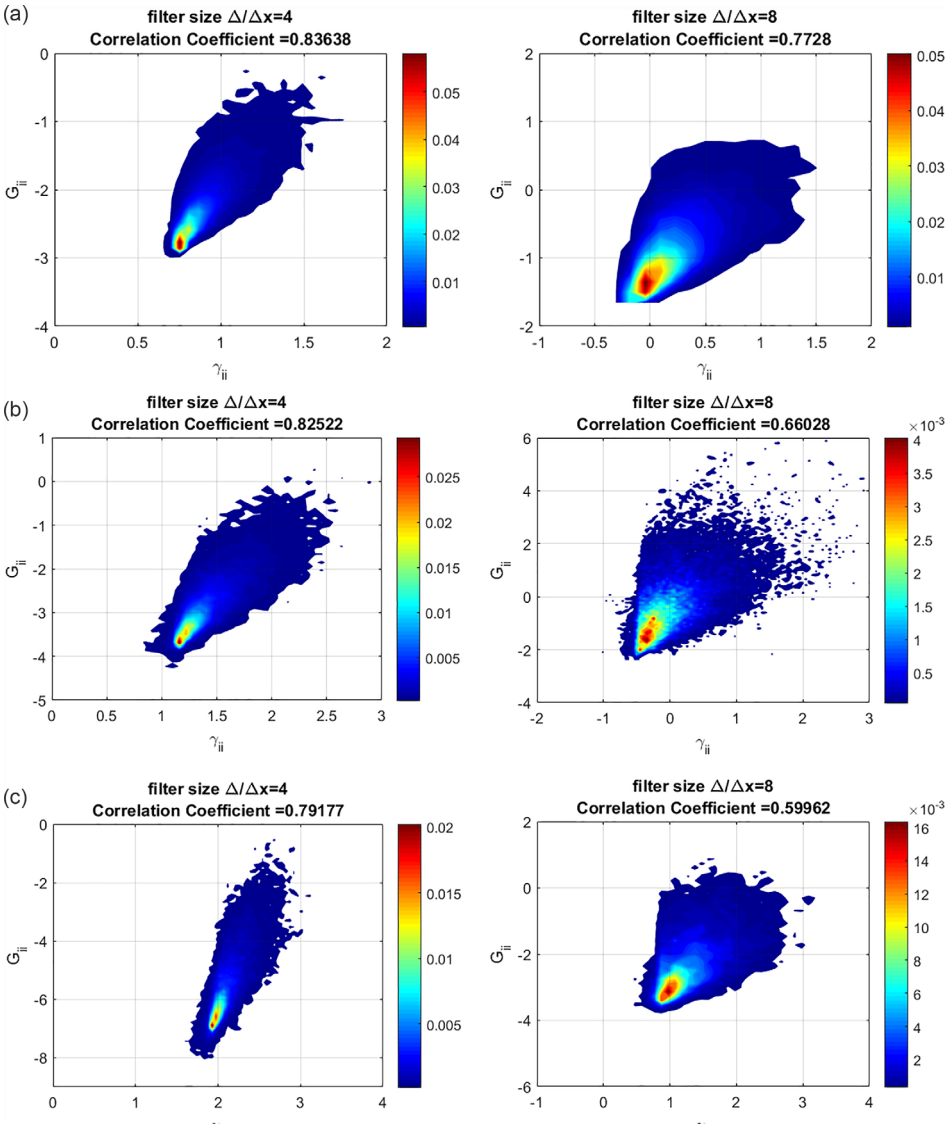

FIG. 5. JPDF between the trace of SGS polymer stretching terms γ_{ii} and G_{ii} normalized by their root mean square obtained from DNS at (a) $Wi = 1.1$, (b) 2.2, and (c) 3.3 with filter sizes $\Delta/\Delta x = 4$ (left column) and $\Delta/\Delta x = 8$ (right column). All data are from the jet centerline ($y/H = 0$) in the range $10 \leq x/H \leq 18$.

points. For clarity, only data from 30 (x, y) points are shown, but we observe a similar behavior when considering all points in that region. It is not shown here for conciseness, but hypothesis **H2** remains valid when comparing individually $\langle \psi_{ij} \rangle$ with $\langle C_{aij} \rangle$.

Figures 4(a)–4(c) show the probability density function (PDF) of ψ_{ii} and γ_{ii} at the self-similar region of the turbulent viscoelastic jet for $W_i = 1.1$, 2.2, 3.3, respectively, for a filter size equal to $\Delta/\Delta x = 4$. These confirm that locally, the quantities of $\psi_{ii} \ll \gamma_{ii}$. As shown, the skewness of γ_{ii} is also significantly more intense than that of ψ_{ii}, so $\langle \gamma_{ii} \rangle_{z-direction} \neq 0$, whereas $\langle \psi_{ii} \rangle_{z-direction} \approx 0$. Masoudian *et al.*[46] and Ferreira *et al.*[37] also reported that ψ_{ii} is negligible in DNS of turbulent channel flows and forced isotropic turbulence of FENE-P fluids, respectively. Therefore, the comparison shows that the SGS of polymer stretching γ_{ii}, or γ_{ij}, cannot be ignored.

It is also observed in Fig. 4 that by increasing Wi, not only the skewness of the polymer stretching SGS, but also the tendency of having negative quantities of it, both increase. The same behavior was observed and reported by Ferreira *et al.*[37] and interpreted there as a sign of the formation of the polymer induced energy cascade at larger Wi number, which was explained in detail by Ref. 40.

C. Scale-similarity of the subgrid-scale polymer stretching: Hypothesis H3

One of the main characteristics of turbulent flows is the existence of self-similarity in the inertial range of scales, which allows the computation of a given subgrid-scale quantity by assessing the same quantity defined at a nearby scale.[65] This assumption has been previously used in the development of many SGS models for Newtonian turbulent flows[28] and prompted Ferreira *et al.*[37] to develop the DSIM model for γ_{ij} in Eq. (22) in isotropic turbulence by applying this concept to the computation of the SGS polymer stretching term. It is important

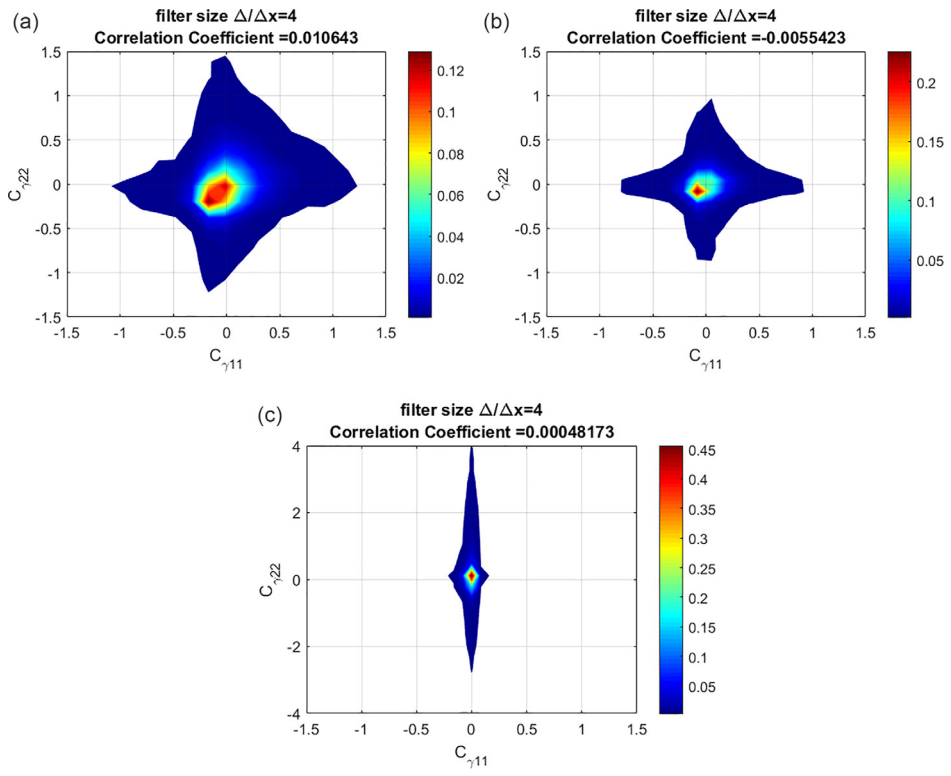

FIG. 6. JPDF between the $C_{\gamma 11}$ and $C_{\gamma 22}$ [calculated from Eq. (34)] obtained from DNS at (a) $Wi = 1.1$, (b) 2.2, and (c) 3.3 with a filter size $\Delta/\Delta x = 4$. All data are from the jet centerline ($y/H = 0$) in the range $10 \leq x/H \leq 18$.

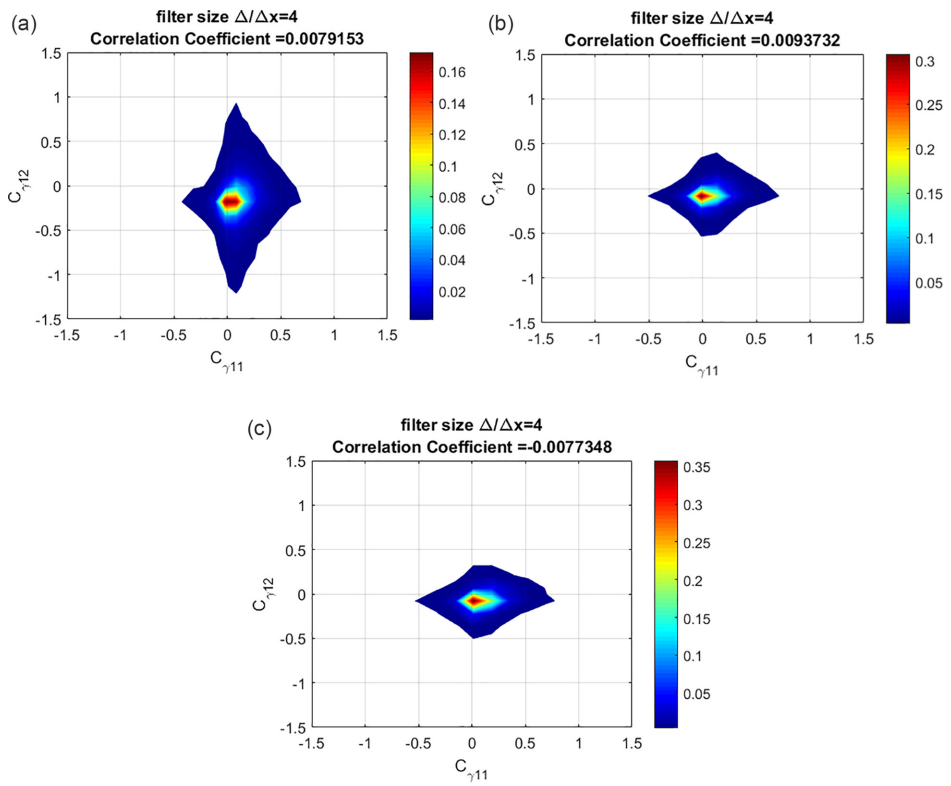

FIG. 7. JPDF between the $C_{\gamma 11}$ and $C_{\gamma 12}$ [calculated from Eq. (34)] obtained from DNS at (a) $Wi = 1.1$, (b) 2.2, and (c) 3.3 with a filter size $\Delta/\Delta x = 4$. All data are from the jet centerline ($y/H = 0$) in the range $10 \leq x/H \leq 18$.

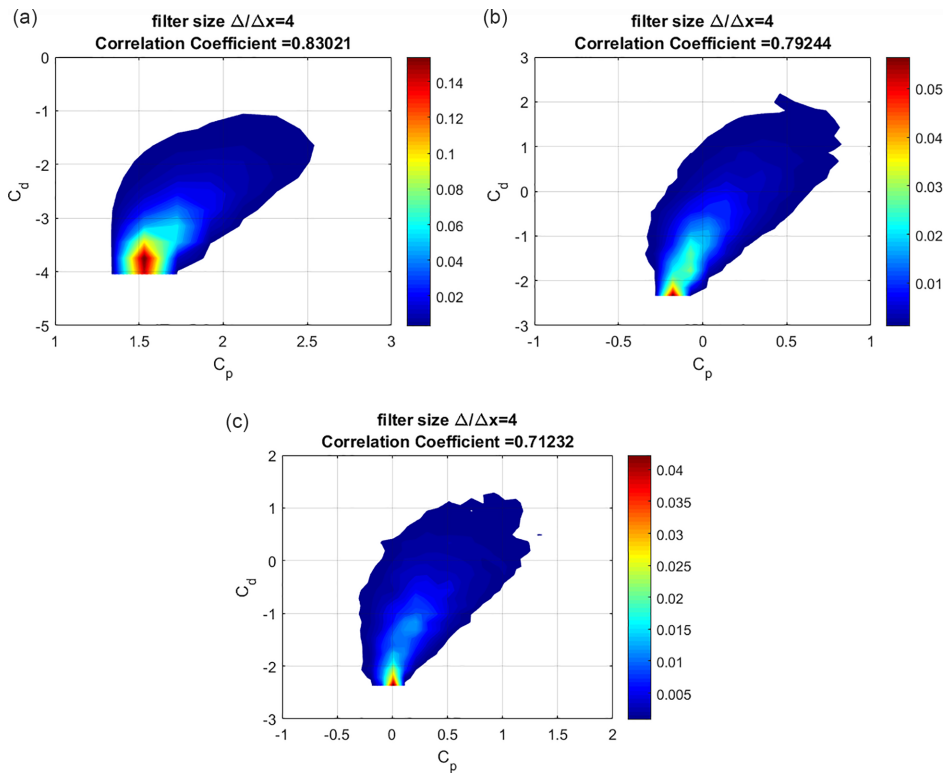

FIG. 8. JPDF functions between polymer stretching C_p and dissipation C_d terms of the trace of the filtered conformation tensor evolution equation obtained from DNS at (a) $Wi = 1.1$, (b) 2.2, and (c) 3.3 with a filter size $\Delta/\Delta x = 4$. All data are from the jet centerline ($y/H = 0$) in the range $10 \leq x/H \leq 18$.

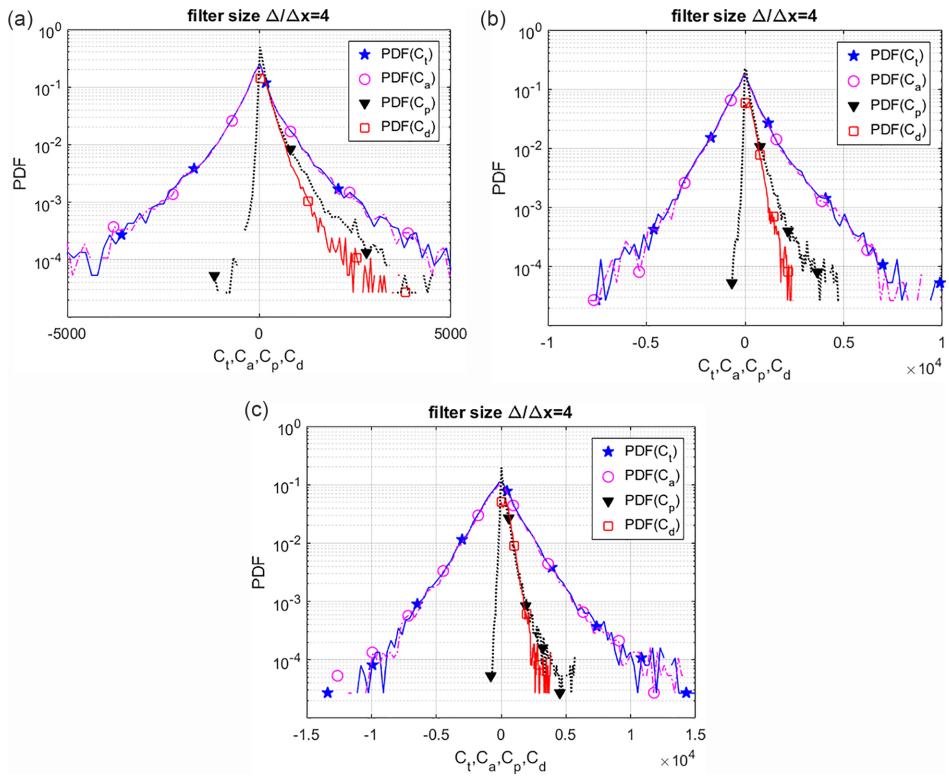

FIG. 9. PDF of the traces of C_t, C_a, C_p, and C_d at (a) $Wi = 1.1$, (b) 2.2, and (c) 3.3 for a filter size $\Delta/\Delta x = 4$. All data are from the jet centerline ($y/H = 0$) in the range $10 \leq x/H \leq 18$. Lines are a guide to the eye.

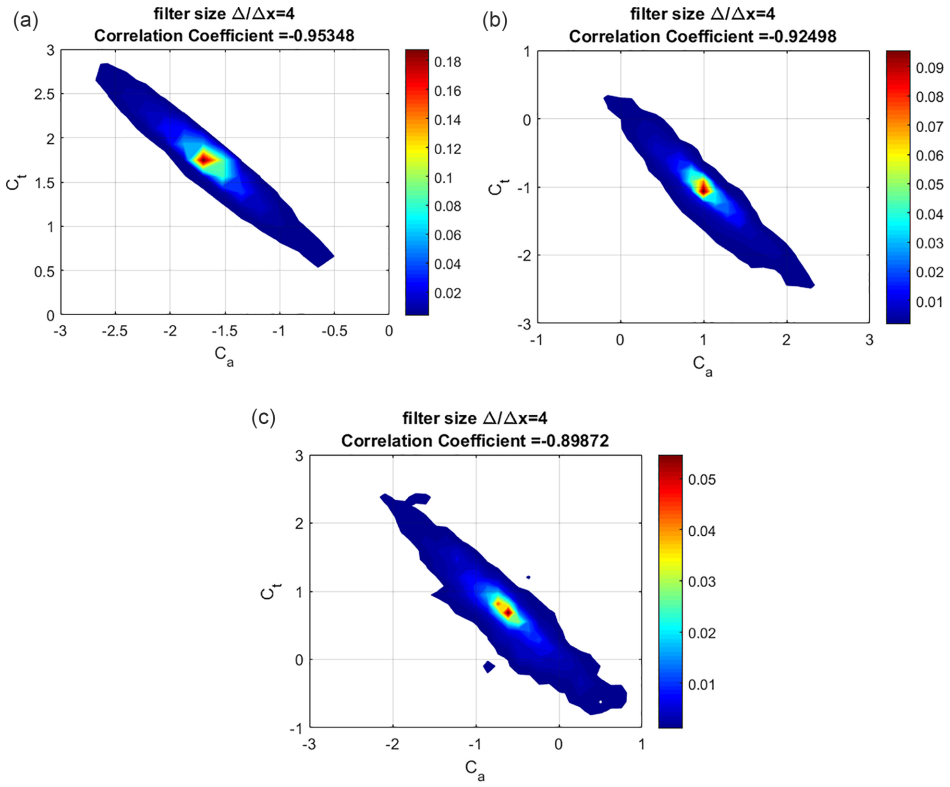

FIG. 10. JPDF functions between temporal C_t and advection C_a terms from the trace of the conformation tensor transport, obtained from DNS at (a) $Wi = 1.1$, (b) 2.2, and (c) 3.3 with a filter size $\Delta/\Delta x = 4$. All data are from the jet centerline ($y/H = 0$) in the range $10 \leq x/H \leq 18$.

to assess this assumption in the present inhomogeneous flow configuration. Specifically, the self-similarity of subgrid-scales was originally proposed by Bardina *et al.*,[66] for the SGS stress tensor of the momentum equation. The model assumes that the SGS stress (for a Newtonian fluid) can be approximated by

$$\tau_{ij}^{sgs} = c\left(\widetilde{\bar{u}_i \bar{u}_j} - \widetilde{\bar{u}}_i \widetilde{\bar{u}}_j\right), \tag{31}$$

where C is a constant of order $O(1)$, and $\widetilde{\Delta}$ is the width of the test filter, often taken as having twice the width of the original filter. By applying this concept to the subgrid-scale polymer stretching term [γ_{ij} in Eq. (22)], the subgrid-scale polymer stretching at the test filter width is

$$G_{ij} = \left[\widetilde{\frac{\partial u_i}{\partial x_k} C_{jk}} - \frac{\partial \widetilde{u}_i}{\partial x_k} \widetilde{C}_{jk}\right] + \left[\widetilde{\frac{\partial u_j}{\partial x_k} C_{ik}} - \frac{\partial \widetilde{u}_j}{\partial x_k} \widetilde{C}_{ik}\right]. \tag{32}$$

By considering the self-similarity of the subgrid-scales computed at filter widths Δ and $\widetilde{\Delta}$, (here we take $\widetilde{\Delta} = 2\Delta$) the SGS of polymer stretching tensor is calculated by

$$\gamma_{ij} = C_\gamma G_{ij}, \tag{33}$$

where C_γ is a numerical coefficient that needs to be computed. This constitutes the assumption **H3** used by Ferreira *et al.*[37] in homogeneous turbulence.

To assess this assumption in the turbulent jet flow configuration, Figs. 5(a)–5(c) show the joint probability density functions (JPDFs) of the trace of the SGS polymer stretching terms γ_{ii} and G_{ii} with $Wi = 1.1$, 2.2, and 3.3 and for filter size $\Delta/\Delta x = 4$ and 8.

The two quantities are clearly correlated, and the correlation coefficient between γ_{ii} and G_{ii} varies between 0.83 and 0.599, so of order 1, depending on the filter size and Wi number. Specifically, the correlation coefficient decreases when increasing Wi and the filter size, which is similar to the behavior and values described in Ferreira *et al.*[37] The correlation coefficients and shape of the PDFs attest that the scale-similarity assumption (**H3**) is also valid for inhomogeneous free shear flows and can be used in the development of SGS closures.

The closure in Eq. (31) has the same coefficient for all tensor components, i.e., it is an isotropic model, still to be determined. As in Ferreira *et al.*[37] we now investigate the possibility of using anisotropic model coefficients $C_{\gamma_{ij}}$, defined by a rewriting of assumption **H3** as

$$\gamma_{ij} = C_{\gamma ij} G_{ij} (\text{no summation on } i \text{ and } j). \tag{34}$$

To investigate this issue, Figs. 6 and 7 show the JPDF between $C_{\gamma 11} = \frac{\gamma_{11}}{G_{11}}$ and $C_{\gamma 22} = \frac{\gamma_{22}}{G_{22}}$, and between $C_{\gamma 11} = \frac{\gamma_{11}}{G_{11}}$ and $C_{\gamma 12} = \frac{\gamma_{12}}{G_{12}}$, respectively, for filter size $\Delta/\Delta x = 4$.

As in Ferreira *et al.*[37] for homogeneous turbulence, the figures clearly show that the correlation coefficients between $C_{\gamma 11}$ and $C_{\gamma 22}$ and between $C_{\gamma 11}$ and $C_{\gamma 12}$ are approximately zero. This means that these quantities are statistically independent, which validates the assumption of using an isotropic C_γ in the DSIM SGS model, also for the inhomogeneous flow configuration used in the present work. For other combinations of coefficients not shown, the correlation coefficient was equally very small.

D. Local equilibrium of the polymeric elastic energy and statistically stationary flow: Hypothesis H4, H5, and H6

We now investigate the hypothesis used by Ferreira *et al.*[37] to compute the model constant C_γ, defined in Eq. (34). By using Eq. (29) and by employing the condition of statistical stationarity and homogeneity Ferreira *et al.*[37] arrived at the following expression:

$$\left\langle 2\overline{\frac{\partial u_i}{\partial x_k}C_{ik}}\right\rangle = \left\langle \frac{1}{\lambda}\left[\overline{f(C_{kk})C_{ii}} - \delta_{ii}\right]\right\rangle, \tag{35}$$

where the brackets $\langle\rangle$ denote an ensemble averaging operation which was performed in all three homogeneous directions in the homogeneous isotropic turbulence configuration of Ferreira *et al.*.[37] In such context, this expression represents the "global" equilibrium of the resolved elastic energy, i.e., in statistically stationary isotropic turbulence the elastic energy produced by the interaction between the polymer molecules and the turbulent velocity fluctuations is balanced by its transfer into the polymer molecules where it is stored as elastic energy, so that the total (resolved) elastic energy-which is proportional to $\overline{C}_{kk} = \overline{C}_{xx} + \overline{C}_{yy} + \overline{C}_{zz}$-remains constant. We denote this assumption as **H4**.

It is important to clarify how this assumption can be used in the context of the present flow configuration since it is clear that in turbulent jet flows, as well as in other inhomogeneous flow configurations, Eq. (35) will not be exactly verified. Hence, one needs to assess how this expression, or some sort of variant of it, can be used in order to extend the DSIM model into free shear flows.

We start by noting that statistical stationarity in the far field (fully developed) region of the jet allows one to write also

$$\left\langle \frac{\partial \overline{C}_{ii}}{\partial t}\right\rangle = 0, \tag{36}$$

(we denote this assumption by **H5**). The brackets still refer to averaging in the homogeneous direction, which in the present context is the z-direction. By averaging Eq. (29) and considering a negligible $\langle\psi_{ii}\rangle$ (**H2**), together with the self-similarity assumption for the SGS polymer stretching term (**H3**), this equation can be written as

$$\left\langle \overline{u}_k\frac{\partial \overline{C}_{ii}}{\partial x_k}\right\rangle = \left\langle 2\frac{\partial \overline{u}_i}{\partial x_k}\overline{C}_{ik}\right\rangle - \left\langle \frac{1}{\lambda}\left[\overline{f(C_{kk})}\overline{C}_{ii} - \delta_{ii}\right]\right\rangle + \langle C_\gamma G_{ii}\rangle. \tag{37}$$

Notice that the term on the LHS of Eq. (37) is the mean advection of the trace of the conformation tensor, which is rigorously zero in isotropic turbulence due to the homogeneity of the flow, but has to be retained in inhomogeneous turbulent flows, such as in turbulent viscoelastic jets. However, it is likely that this term is negligible compared to the other terms. Indeed, whereas the advection of $\overline{C}_{ii}$ is clearly associated with the largest scales of motion in the jet, the terms representing the production and dissipation of $\overline{C}_{ii}$—the first and second terms on the RHS of Eq. (37)—are governed by the smallest scales of the flow. We denote this assumption (neglecting the advection of $\overline{C}_{ii}$) by **H6**. We can therefore use an expression similar to the one used by Ferreira *et al.*[37] for the determination of the model constant C_γ, with only minor corrections related to the averaging procedure.

By inserting all the aforementioned hypotheses into Eq. (37), the model constant C_γ can be obtained from the following expression:

$$C_\gamma = \frac{\left\langle \frac{1}{2\lambda}\left[\overline{f(C_{kk})C_{ii}} - \delta_{ii}\right]\right\rangle_z - \left\langle \frac{\partial \bar{u}_i}{\partial x_k}\bar{C}_{ik}\right\rangle_z}{\left\langle \widetilde{\frac{\partial u_i}{\partial x_k}C_{ik}} - \frac{\partial \widetilde{u}_i}{\partial x_k}\widetilde{C}_{ik}\right\rangle_z}, \tag{38}$$

where the averaging procedure now consists on a spatial average carried out along the only flow direction where the flow is homogeneous (z-direction).

Hypothesis **H5** does not need to be assessed as it stems directly from the concept of statistical stationarity, whereas hypothesis **H4** and **H6** are somehow related and need to be assessed simultaneously.

In order to assess hypothesis **H4**–**H6** dealing with local equilibrium assumption, Fig. 8 shows the joint probability density functions (JPDFs) of the polymer stretching (C_p) and dissipation (C_d) of the trace of the conformation tensor defined in Eq. (29), for $Wi = 1.1$, 2.2, and 3.3 and filter size $\Delta/\Delta x = 4$. The correlation coefficients between C_p and C_d are very high, at 0.84, 0.79, and 0.71 for $Wi = 1.1$, 2.2, and 3.3, respectively, with $\Delta/\Delta x = 4$. This confirms that, as in isotropic turbulence, C_p and C_d are in approximately local equilibrium, even though the correlation coefficient slightly decreases with increasing Wi numbers.

To complete the assessment of the **H4**–**H6** assumptions, it is important to shown that the other terms of Eq. (29) (terms C_t and C_a) are negligible in comparison with C_p and C_d terms.

Figure 9 shows the probability distribution functions of all terms of Eq. (29) (C_t, C_a, C_p, and C_d) for $\Delta/\Delta x = 4$ and $Wi = 1.1$, 2.2, and 3.3. The PDF of C_t and C_a is symmetric which explains why the local value of the sum of these quantities is approximately 0. Finally, Fig. 10 shows the joint probability density functions between temporal variation C_t and advection terms C_a of the trace of the conformation tensor, for $Wi = 1.1$, 2.2, and 3.3 and filter size $\Delta/\Delta x = 4$. The correlation coefficient between C_t and C_a is equal to −0.95, −0.94, and −0.92, which finally confirms that all hypotheses **H4**, **H5**, and **H6** are verified.

To summarize, all the *a priori* tests conducted in the reference DNS of turbulent viscoelastic jets clearly show that all the assumptions used by Ferreira *et al.*[37] in the development of the DSIM model in isotropic turbulence are also valid in the present inhomogeneous free turbulent flow configuration, and are likely valid in other free shear flows of viscoelastic fluids such as wakes and mixing layers. In Sec. VI, we assess the combination of all closures through *a posteriori* (LES) tests.

VI. *A POSTERIORI* TESTS: LES OF TURBULENT PLANAR JET FENE-P FLUID

Several LES of turbulent planar jet flow of FENE-P fluid were performed with the various closures presented, including the Smagorinsky and dynamic Smagorinsky models for the SGS term of momentum equation and the DSIM model for the SGS polymer stretching term in the conformation tensor equation. The results are assessed against the reference DNS of Guimarães *et al.*[47] in what are typically called *a posteriori* tests. The comparisons confirm that the DSIM model, in its original formulation and, in particular, in combination with the dynamic Smagorinsky closure for the SGS stress, performs well in planar turbulent jets, and arguably the same should be true for other free shear flows. Incidentally, we did also some tests using the Vreman[68] and the shear improved Smagorinsky[69] closures for the SGS stress, but no advantages were observed relative to the

dynamic Smagorinsky model; therefore, for the sake of conciseness, such results are neither presented nor those closures introduced.

The LES were carried out with the same numerical code used in Guimarães *et al.*[47] and the physical and computational parameters are chosen as close as possible to those of the reference DNS, naturally using coarser grids than in the DNS.

The amplitude of noise for all inlet velocity fluctuations was set at 10%, as in Guimarães *et al.*;[47] however, the ratio between the inlet slot-width and momentum thickness was set to $H/\theta = 15$,[47,49] to avoid the Gibbs phenomena that could arise with the coarser grids used in LES. In the following, we use subscripts "N" (Newtonian fluid), "Sm" (Smagorinsky), and "Dyn" (dynamic Smagorinsky) to denote the various subgrid-scale stress closures used in the computation. Subscript "f" represents a second LES carried out using a finer grid. The main details of the simulations are summarized in Table II, where the reported values of A_δ, A_{U_c}, A_{σ_c} were obtained using the dynamic Smagorinsky model.

In all simulations and similarly to the DNS of Guimarães *et al.*,[47] the Reynolds number was equal to $Re = 3500$, and the ratio of the solvent to total viscosity and the maximum dumbbell extensibility were equal to $\beta_s = 0.8$ and $L^2 = 10^4$, respectively. The domain size was $L_x = 19.2H$, $L_y = 24\,H$ in the streamwise and normal directions, and $L_z = 6H$ in the spanwise direction, for a "normal" grid size with $192 \times 192 \times 48$ grid points, and a "finer" grid size with $256 \times 256 \times 64$ points. By considering $\lambda = 0.3$, 0.6, 0.9 s, the global Weissenberg number became equal to $Wi = 1.1$, 2.2, 3.3.

A. Instantaneous vorticity and trace of conformation tensor field

Figures 11(a)–11(d) show contours of instantaneous vorticity magnitude normalized by $\left(U_J - U_\infty^{in}\right)/H$ in the (x,y) plane of the turbulent planar jet obtained by LES for Newtonian and viscoelastic flows at Weissenberg numbers, $Wi = 1.1$, 2.2, 3.3. These results were obtained in the finer grid (LES_f) and used the dynamic Smagorinsky model.

The Newtonian contours in Fig. 11(a) are very similar to those shown in Guimarães *et al.*,[47] for the same physical conditions. Kelvin–Helmholtz vortices emerge at about at $x/H \approx 4$ for all simulations and tend to break up into smaller-scale eddies after about $x/H \approx 6$. By about $x/H \approx 10$–12, the flow seems to have attained the typical features of fully developed turbulence, with a clear display of many small-scale eddies without any preferential direction. As reported by Guimarães *et al.*[47] and the other extensive studies on turbulent viscoelastic fluids,[69–72] the main effects of increasing the Wi number in the turbulent planar jet structure are (i) a significant suppression of small-scale turbulent motions (compared to the Newtonian reference case), with a concomitant considerable reduction of the vorticity magnitude as observed by the range of values of $|\omega^+|$ obtained, (ii) the elongation of the eddy structures, and (iii) a reduction of the jet spreading rate. All of these features are clearly shown in Fig. 11. The effect of polymers on the dampening of the vorticity magnitude can be well appreciated in these figures since increasing Wi from 0 (Newtonian) to 3.3 causes the maximum vorticity magnitude to decrease from $|\omega^+|_{\max} = 9.15$ for the LES of the Newtonian fluid to 4.55 for the LES of FENE-P fluid. Simultaneously, the coherent structures become more elongated and spread at a lower rate. Similar observations were reported in Guimarães *et al.*[47] and many experimental studies, e.g., Refs. 73–77.

As the detailed investigations of forced homogeneous isotropic turbulence have shown[39,40] the increase in Wi leads to a situation in which the polymer timescale becomes larger than the Kolmogorov scale. Further increases in Wi result in a deviation of the large to small scale turbulent kinetic energy transfer from the classical mechanism to a polymer induced cascade mechanism. This is seen through both reductions of vorticity and of small scale turbulent motion (at the same level of vorticity). As has been previously observed in inhomogeneous wall turbulence,[12,13,69–72] and is also seen in this jet flow,[47] these features and the strain hardening of some fluid properties, such as the fluid extensional viscosity, lead to stronger reductions in transverse and spanwise turbulence than in streamwise turbulence and the enhanced turbulence anisotropy translates into more elongated structures.

Figure 12 shows contours of the trace of conformation tensor $\mathrm{tr}(C)$ which is proportional to the elastic energy stored by the stretched polymer molecules, for $Wi = 1.1$, 2.2, and 3.3, at the mid-plane of the computational domain ($z = 0$), and at the same instant of time of Fig. 11. To help the visualizations, the range of the color maps was taken to be much lower than maximum $\mathrm{tr}(C)$ for all cases. Maxima of $\mathrm{tr}(C)$ occurs in the transitional region, and when approaching the far field $\mathrm{tr}(C)$ decreases. Similarly to other studies, e.g., Valente *et al.*[39] and Guimarães *et al.*,[47] it was observed that even for the most extreme scenario ($Wi = 3.3$), $\mathrm{tr}(C)_{\max} \approx 4500$ in the fully developed turbulence region (at $x/H \approx 14$) corresponding to $\mathrm{tr}(C)_{\max}/L^2 = 0.45$. However, inspection of the instantaneous fields shows that the probability of having local values of $\mathrm{tr}(C)_{\max}/L^2$ is very low, and generally those values remain $\mathrm{tr}(C)_{\max}/L^2 \ll 1$.

TABLE II. Summary of physical and computational features of LES used in the *a posteriori* tests with domain size $\frac{L_x \times L_y \times L_z}{H^3} = 19.2 \times 24 \times 6$.

	Wi	λ(s)	β_s	L	Grid points	A_δ	A_{U_c}	A_{τ_c}
LES_N	0	0	1.0	NA	$192 \times 192 \times 48$	0.124	0.165	NA
$LES_{1.1}$	1.1	0.3	0.8	100	$192 \times 192 \times 48$	0.108	0.169	1.8
$LES_{2.2}$	2.2	0.6	0.8	100	$192 \times 192 \times 48$	0.090	0.156	0.63
$LES_{3.3}$	3.3	0.9	0.8	100	$192 \times 192 \times 48$	0.084	0.155	0.34
LES_{Nf}	0	0	1.0	NA	$256 \times 256 \times 64$	0.124	0.180	NA
$LES_{1.1f}$	1.1	0.3	0.8	100	$256 \times 256 \times 64$	0.122	0.187	1.65
$LES_{2.2f}$	2.2	0.6	0.8	100	$256 \times 256 \times 64$	0.094	0.167	0.57
$LES_{3.3f}$	3.3	0.9	0.8	100	$256 \times 256 \times 64$	0.085	0.154	0.38

B. Classical statistics

In this section, we analyze the statistical quantities obtained from the several LES carried out with the combined dynamic Smagorinsky and DSIM models by comparing them with the statistics obtained in the reference DNS.[46] In some simulations, the classical Smagorinsky model was also used. The comparisons are made in terms of Reynolds-averaged quantities, and for this purpose, the LES and DNS data of this statistically stationary flow are averaged in time and in space in the homogeneous direction. To denote Reynolds-averaged quantities, in this section, we use the overbar, which here does not represent a filtered quantity.

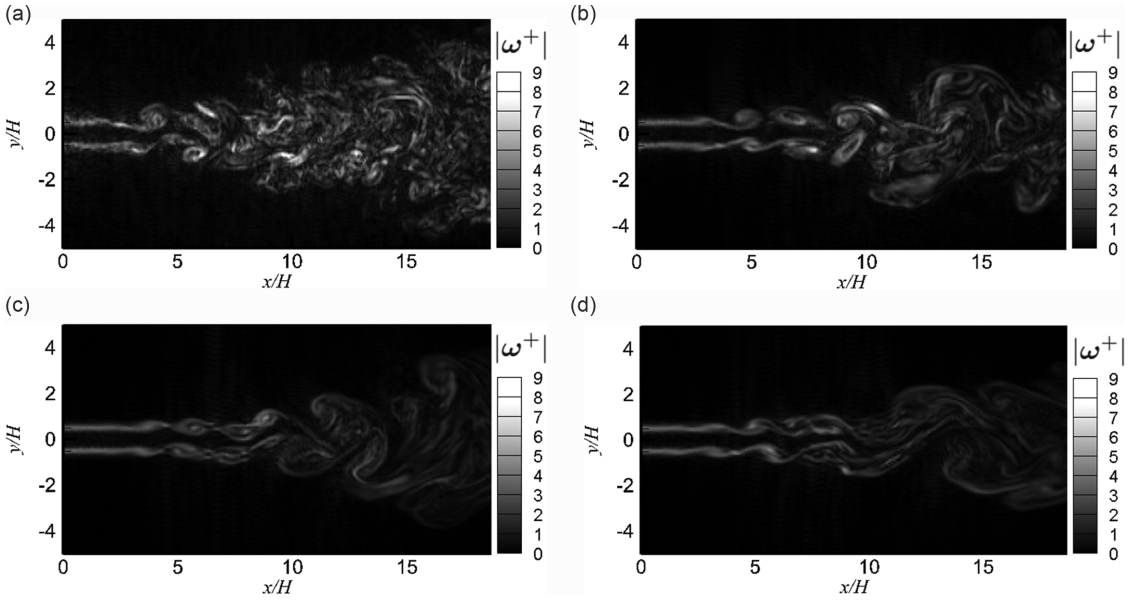

FIG. 11. Contours of instantaneous vorticity normalized by $(U_J - U_\infty^{in})/H$ at the middle plane of the domain ($z = 0$) for (a) Newtonian ($|\omega^+|_{max} = 9.15$) and viscoelastic flows at *Wi* of (b) 1.1, ($|\omega^+|_{max} = 7.65$) (c) 2.2 ($|\omega^+|_{max} = 4.91$), and (d) 3.3 ($|\omega^+|_{max} = 4.55$). The results were obtained in the finer grid (LES_f) using the dynamic Smagorinsky model.

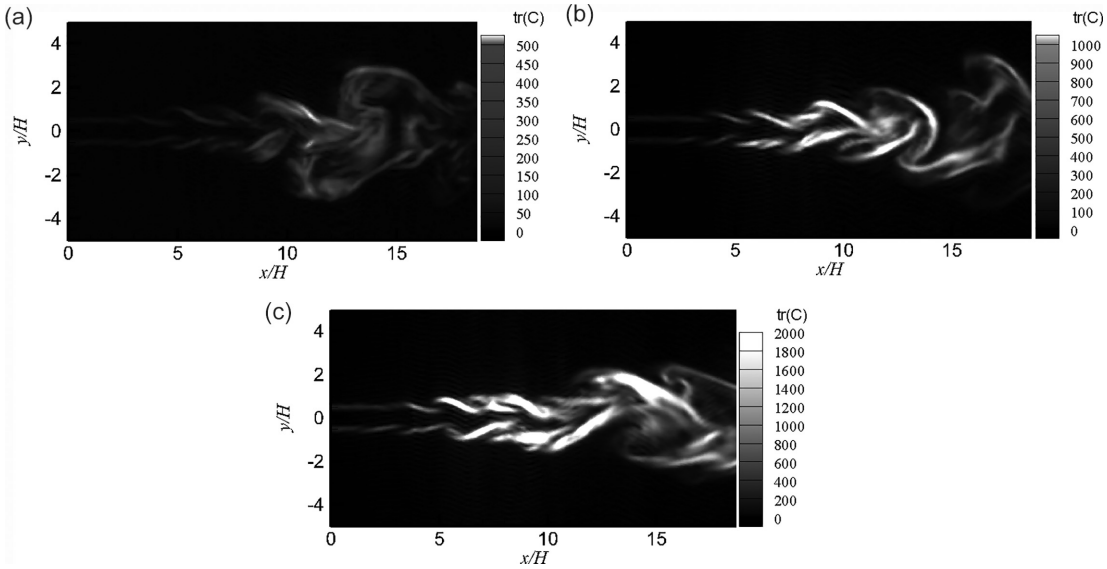

FIG. 12. Contours of the trace of conformation tensor tr(*C*) for (a) $Wi = 1.1$, (b) 2.2, and (c) 3.3 at the mid-plane of the computational domain ($z = 0$), and corresponding to the same instant of time of Figs. 11(b)–11(d). The results were obtained in the finer grid (LES_f) using the dynamic Smagorinsky model.

Guimarães *et al.*[47] showed that in turbulent viscoelastic jets the shear layer thickness $\delta(x)$ and the decay of mean centerline velocity $U_c(x)$ evolve as simple functions of the streamwise distance x

$$\frac{\delta(x)}{H} = A_\delta\left(\frac{x - x_0}{H}\right) \tag{39}$$

and

$$\left(\frac{U_c(x)}{U_J}\right)^{-2} = A_{U_c}\left(\frac{x - x_0}{H}\right), \tag{40}$$

where A_δ and A_{U_c} are constants and x_0 is the virtual jet origin, and that increasing the *Wi* number decreases both the shear layer thickness and the centerline velocity decay rates.

Since fluid viscoelasticity and the subgrid-scale models tend to delay the transition to turbulence, the comparison between the

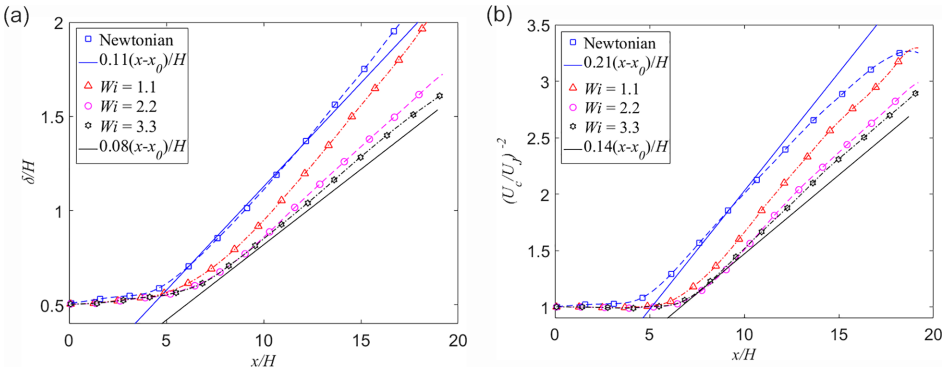

FIG. 13. Evolution of the shear layer thickness (a) and jet centerline velocity decay (b) in LES of turbulent planar jets of Newtonian and FENE-P fluids at $Wi = 1.1$, 2.2, 3.3. Closures used were the dynamic Smagorinsky and DSIM models in the finer grid ($LES_{1.1f}$, $LES_{2.2f}$, and $LES_{3.3f}$) and compared with the reference Newtonian case (LES_{Nf}). Dashed lines connecting symbols are a guide to the eye, and the solid straight lines show the rate laws obtained by DNS at low and high *Wi*.

different models is done through the analysis of the spreading and decay rates, as measured by A_δ and A_{U_c}, and not through the evolution of $\delta(x)$ and $U_c(x)$ from the jet inlet.

Figures 13(a) and 13(b) show the streamwise variation of the jet half-width and centerline velocity decay, respectively, for the simulations carried out with the finer grid. The corresponding values of A_δ and A_{U_c}, in the region $9 \leq x/H \leq 18$, are listed in Table I. The decay rates A_δ and A_{U_c} for the Newtonian LES (LES_{Nf}) are within the ranges of $0.092 \leq A_\delta \leq 0.118$ and $0.093 \leq A_{U_c} \leq 0.220$, that have been reported in previous experimental[78–82] and numerical (DNS)[83] studies, for Newtonian turbulent jets. Regarding the viscoelastic LES and in agreement with the DNS of Guimarães *et al.*,[47] the present LES show that increasing the Weissenberg number postpones the transition to fully developed turbulence and reduces the values of A_δ and A_{U_c} at high *Wi*. Indeed, up to $Wi = 1.1$, the values of A_δ and A_{U_c} remain close to the Newtonian values; however, for $Wi = 2.2$ and 3.3, both A_δ and A_{U_c} are considerably reduced, while still obeying a linear scaling law with $A_\delta = 0.101$, and 0.082, and $A_{U_c} = 0.171$, and 0.160, respectively. Moreover, the results are qualitatively consistent with several experimental studies, e.g., Refs. 84 and 85.

To study the differences from the SGS model used to compute the SGS stresses, Figs. 14 and 15 show the spreading and velocity decay rates, respectively, obtained in the LES of the turbulent jet, using the classical Smagorinsky and the dynamic Smagorinsky models. It is clear that the dynamic Smagorinsky model performs better than the Smagorinsky closure, in particular, for the finer grids.

Figures 16(a)–16(c) also analyze the effect of the SGS stress closures on the transverse profiles of the normalized mean streamwise

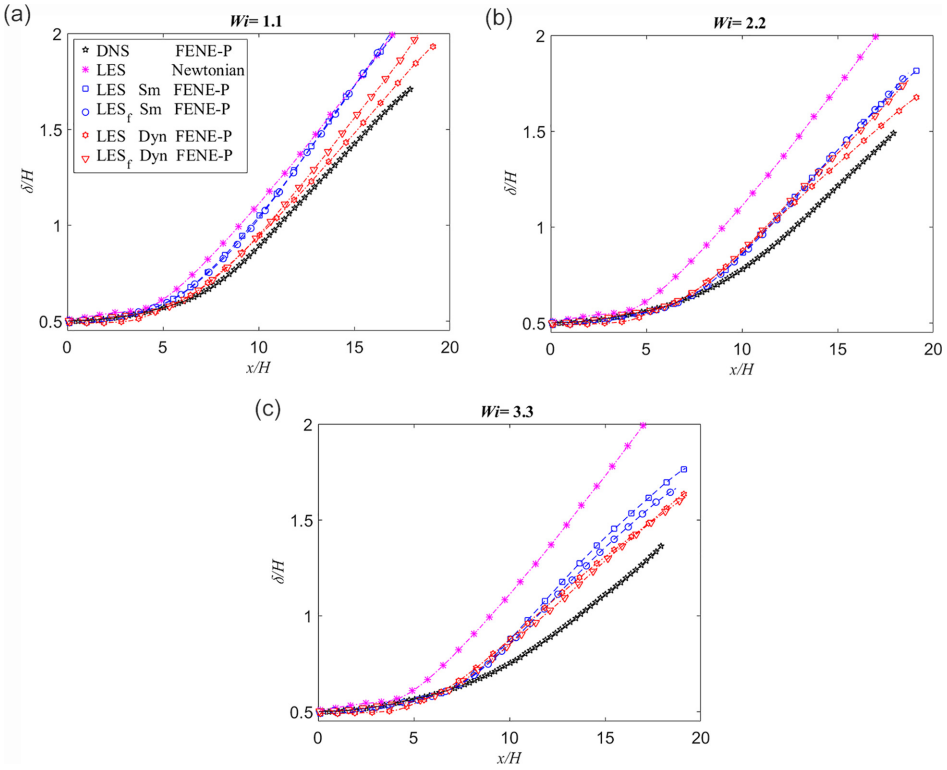

FIG. 14. Effect of the SGS stress model on the evolution of shear layer thickness in the streamwise direction for the turbulent planar jet flows of FENE-P fluid for different SGS stress closures at *Wi* of (a) 1.1, (b) 2.2, and (c) 3.3. The DSIM closure is used for the SGS polymer stretching in the conformation equation and the Smagorinsky (Sm) and dynamic Smagorinsky (Dyn) for the SGS stress in the momentum equation.

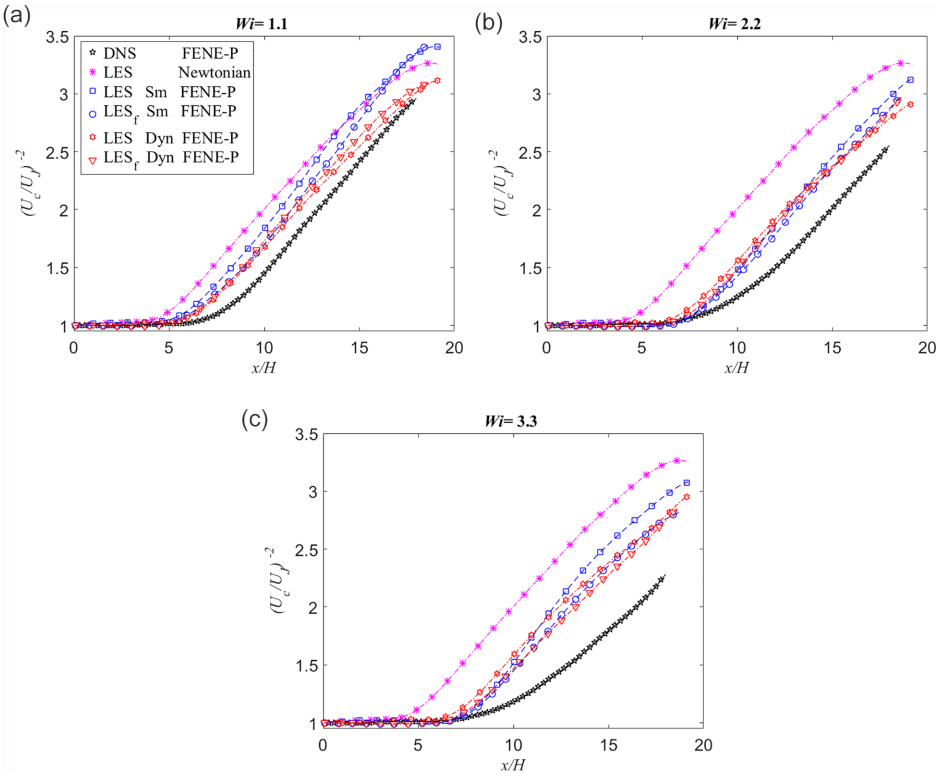

FIG. 15. Effect of SGS stress model on the evolution of jet centerline velocity decay in streamwise direction for the x planar jet flow of FENE-P fluid for different SGS stress closures at Wi of (a) 1.1, (b) 2.2, and (c) 3.3. The DSIM closure is used for the SGS polymer stretching in the conformation equation and the Smagorinsky (Sm) and dynamic Smagorinsky (Dyn) for the SGS stress in the momentum equation.

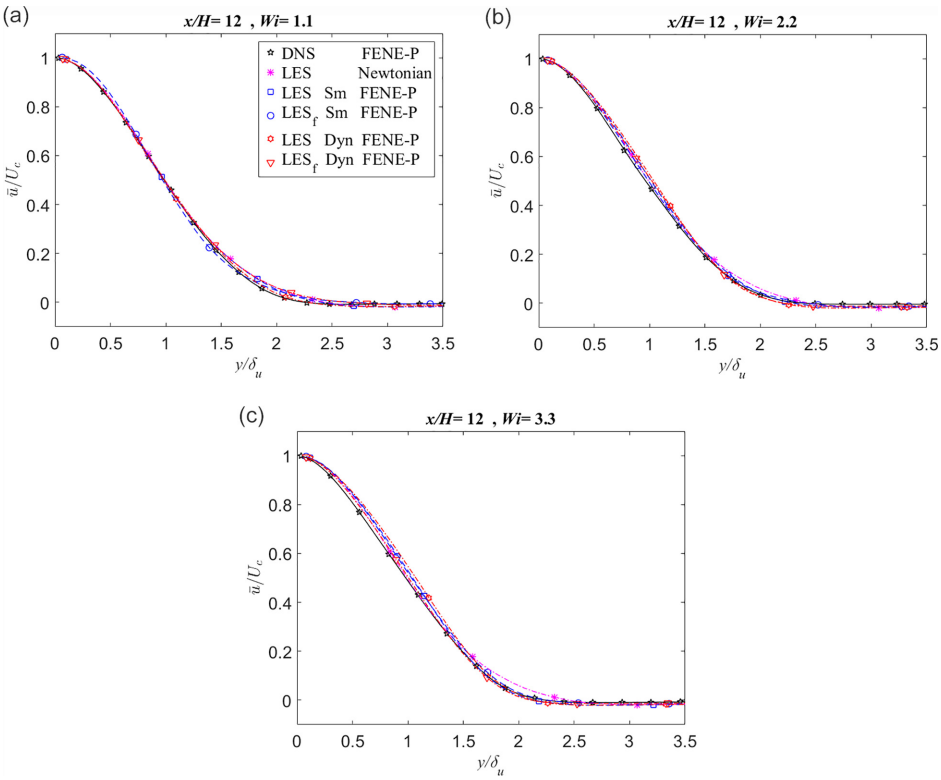

FIG. 16. Effect of SGS stress model on the transverse profiles of streamwise mean velocity normalized by the centerline mean velocity at $x/H = 12$ for Wi of (a) 1.1, (b) 2.2, and (c) 3.3. The DSIM closure is used for the SGS polymer stretching in the conformation equation and the Smagorinsky (Sm) and dynamic Smagorinsky (Dyn) for the SGS stress in the momentum equation.

velocity by comparing these profiles at $x/H = 12$ with the results from the reference DNS. As expected the mean streamwise profiles collapse, which is consistent in the self-similar region of the flow, but with the dynamic Smagorinsky closure performing better than the classical Smagorinsky model (results closer to the DNS data of Ref. 47). Moreover, in agreement with the DNS of Guimarães *et al.*,[47] the effect of increasing Wi number on $\overline{u}/U_c(x)$ is negligible.

Figures 17–19 show the corresponding streamwise evolutions of the normal components of the Reynolds stress tensor on the centerline, here represented as root mean square (rms) of the velocity fluctuations $\sqrt{\overline{u'^2}}$, $\sqrt{\overline{v'^2}}$, and $\sqrt{\overline{w'^2}}$ predicted by LES, and normalized by the mean centerline velocity $U_c(x)$. The figures include data from the reference DNS (Guimarães *et al.*[47]). The rms of the velocity fluctuations of LES follow closely the corresponding DNS results, particularly when the combination of dynamic Smagorinsky and DSIM closures are used. For $Wi \leq 1.1$, the normal Reynolds stresses gradually increase along the transition region to a peak at the beginning of the self-similar region ($x/H \approx 11$), and further downstream their values slightly decrease as the flow attains the fully developed turbulent flow region. However, for $Wi \geq 2.2$, the magnitude of the Reynolds stresses decreases considerably, compared with the turbulent Newtonian jet. Generally speaking, as reported by Guimarães *et al.*,[47] the role of the polymers in the velocity fluctuations can be summarized as postponing the transition to turbulence and by reducing the Reynolds stresses in the self-similar region due to depletion of the small scales of motion caused by a preferential transfer of kinetic energy into the polymer molecules, instead of the classical multi-scale transfer into the solvent via the Richardson–Kolmogorov energy cascade. This tendency to the attenuation of the Reynolds stresses is also reproduced by the present LES, particularly for the combination of the dynamic Smagorinsky and the DSIM model.

Figures 20–22 show the corresponding effects, now on the transverse profiles of the rms of the velocity fluctuations $\sqrt{\overline{u'^2}}$, $\sqrt{\overline{v'^2}}$, and $\sqrt{\overline{w'^2}}$ predicted by LES. These are normalized by the centerline mean velocity $U_c(x)$, and the reference DNS profiles are also shown. In the self-similar region ($x/H = 12$), the rms profiles do not collapse as seen previously with the mean velocity profiles, but are close to the DNS profiles, in particular when relying on the dynamic Smagorinsky for the SGS stress. In all cases the DSIM closure was used for the SGS stretching term in the constitutive equation.

C. Assessment of the self-similar theory of viscoelastic turbulent planar jets

In this section, we assess the performance of LES in the reproduction of the main theoretical results derived by Guimarães *et al.*[47] for the far field region of viscoelastic turbulent planar jets. In their theory, Guimarães *et al.*[47] considered Townsend's hypothesis of self-preservation[86] together with the ideas put forward by Lumley[87] to describe the flow features of turbulent flows of viscoelastic fluids. In short, Lumley[87] defines characteristic velocity (u^*) and length (r^*) scales as

$$u^* = \sqrt{\lambda \varepsilon^s}, \tag{41}$$

$$r^* = \sqrt{\lambda^3 \varepsilon^s}, \tag{42}$$

where ε^s is the mean viscous dissipation rate of the solvent calculated by

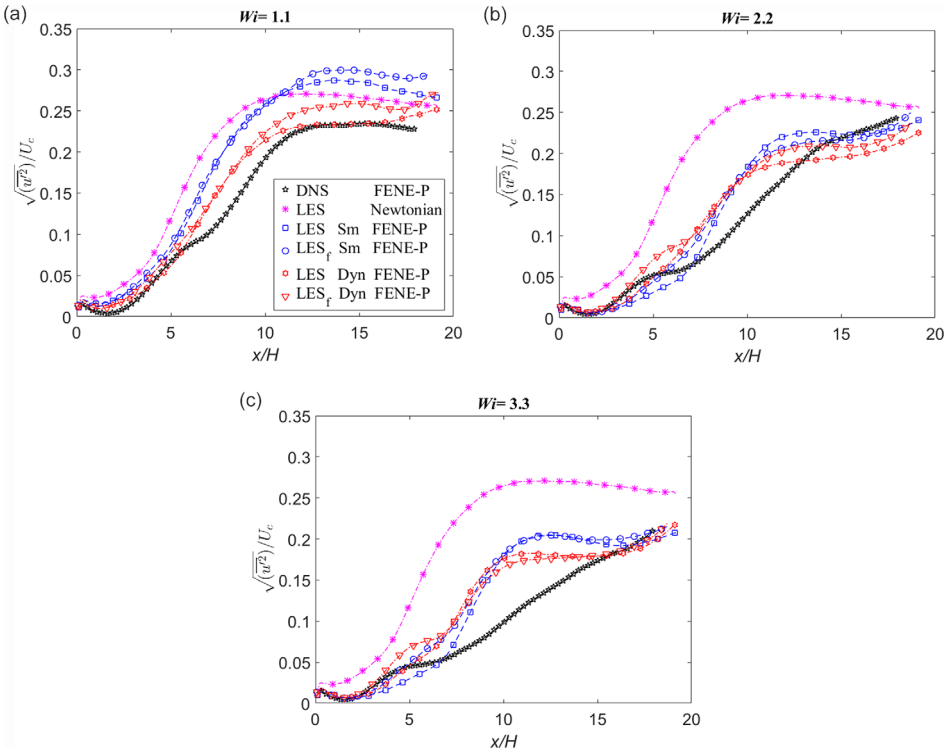

FIG. 17. Effect of SGS stress model on the evolution of the root-mean square of the streamwise velocity fluctuations $\sqrt{\overline{u'^2}}$ along the centerline, normalized by the centerline mean velocity for Wi of (a) 1.1, (b) 2.2, and (c) 3.3. The DSIM closure is used for the SGS polymer stretching in the conformation equation and the Smagorinsky (Sm) and dynamic Smagorinsky (Dyn) for the SGS stress in the momentum equation.

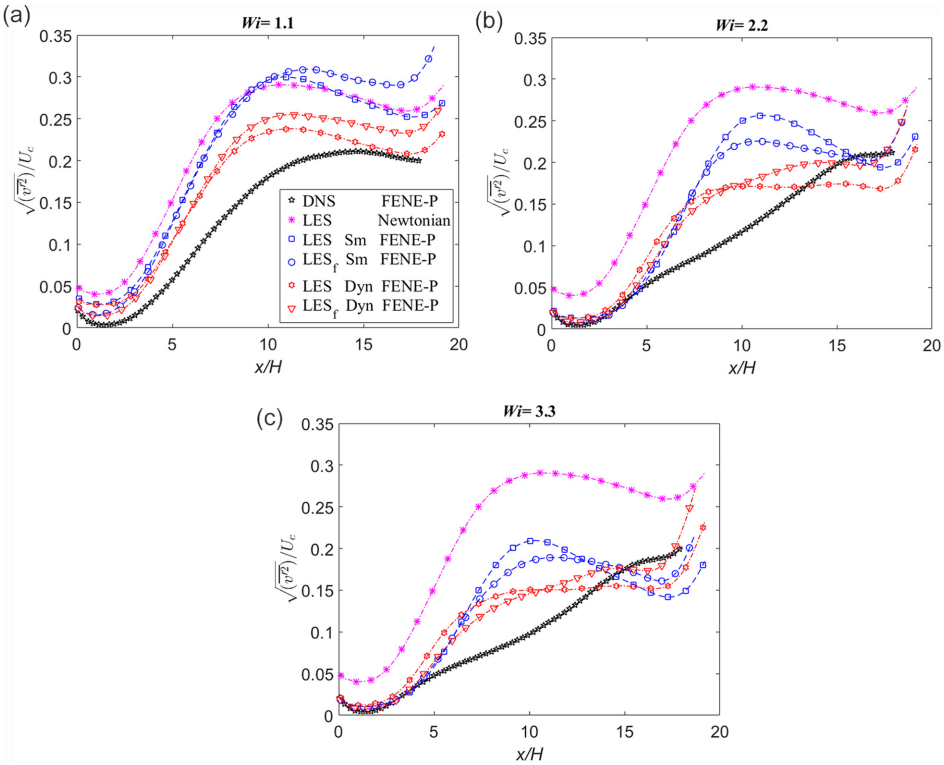

FIG. 18. Effect of SGS stress model on the evolution of the root-mean square of the transverse velocity fluctuations $\sqrt{\overline{v'^2}}$ along the centerline, normalized by the centerline mean velocity for *Wi* of (a) 1.1, (b) 2.2, and (c) 3.3. The DSIM closure is used for the SGS polymer stretching in the conformation equation and the Smagorinsky (Sm) and dynamic Smagorinsky (Dyn) for the SGS stress in the momentum equation.

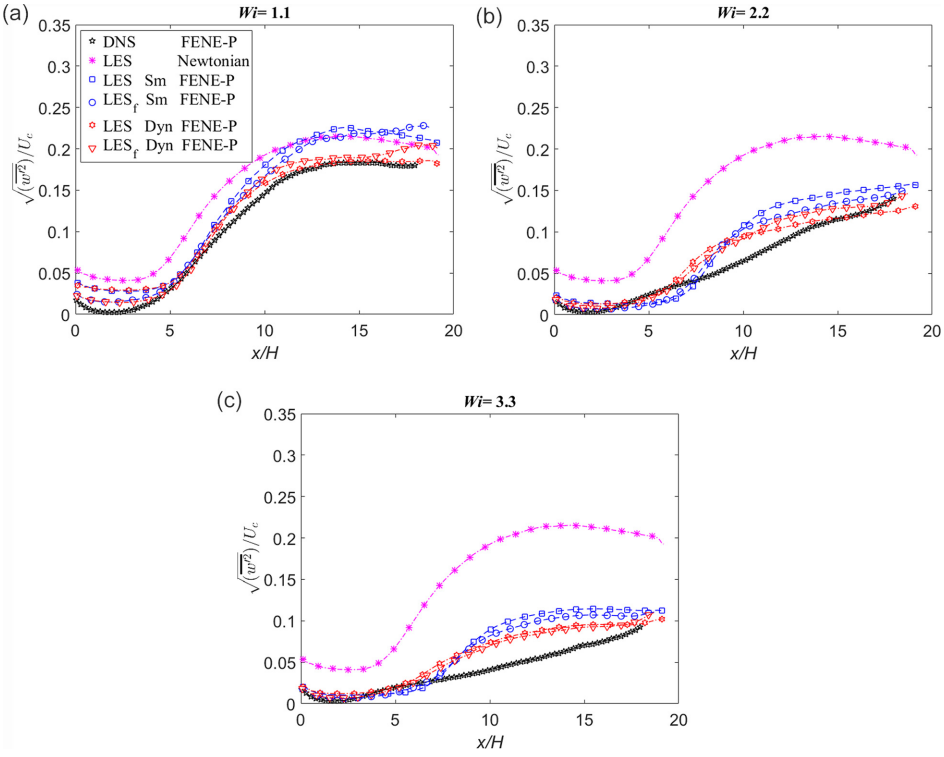

FIG. 19. Effect of SGS stress model on the evolution of the root-mean square of the spanwise velocity fluctuations $\sqrt{\overline{w'^2}}$ along the centerline, normalized by the centerline mean velocity for *Wi* of (a) 1.1, (b) 2.2, and (c) 3.3. The DSIM closure is used for the SGS polymer stretching in the conformation equation and the Smagorinsky (Sm) and dynamic Smagorinsky (Dyn) for the SGS stress in the momentum equation.

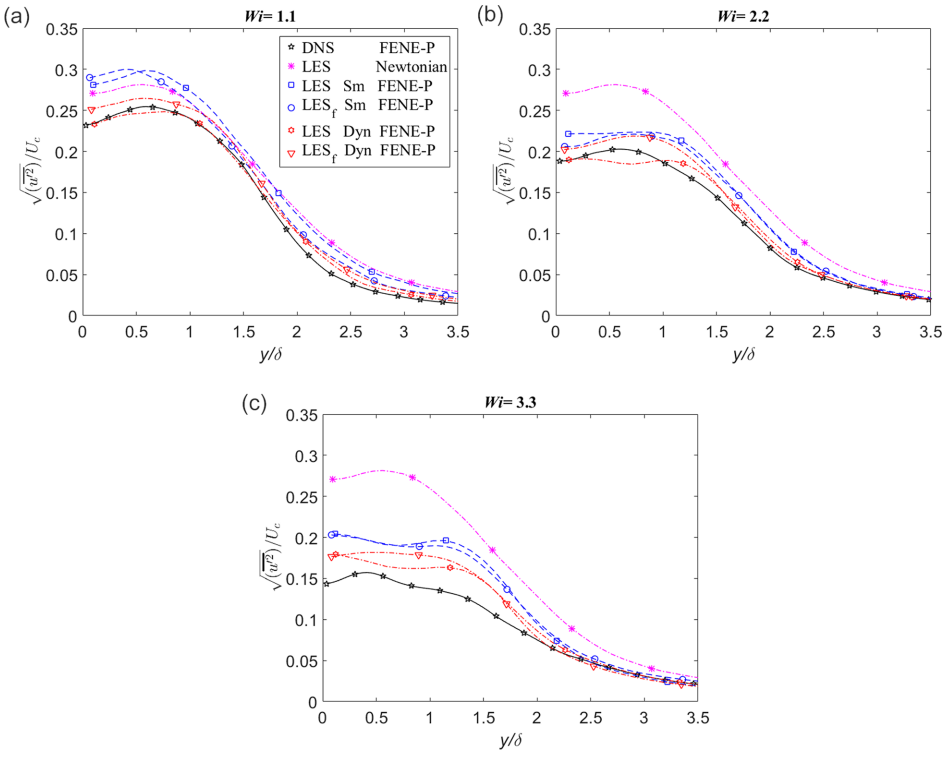

FIG. 20. Effect of SGS stress model on the mean profiles of the rms of the streamwise velocity fluctuations $\sqrt{\overline{u'^2}}$, normalized by the centerline mean velocity, at $x/H = 12$ for Wi of (a) 1.1, (b) 2.2, and (c) 3.3. The DSIM closure is used for the SGS polymer stretching in the conformation equation and the Smagorinsky (Sm) and dynamic Smagorinsky (Dyn) for the SGS stress in the momentum equation.

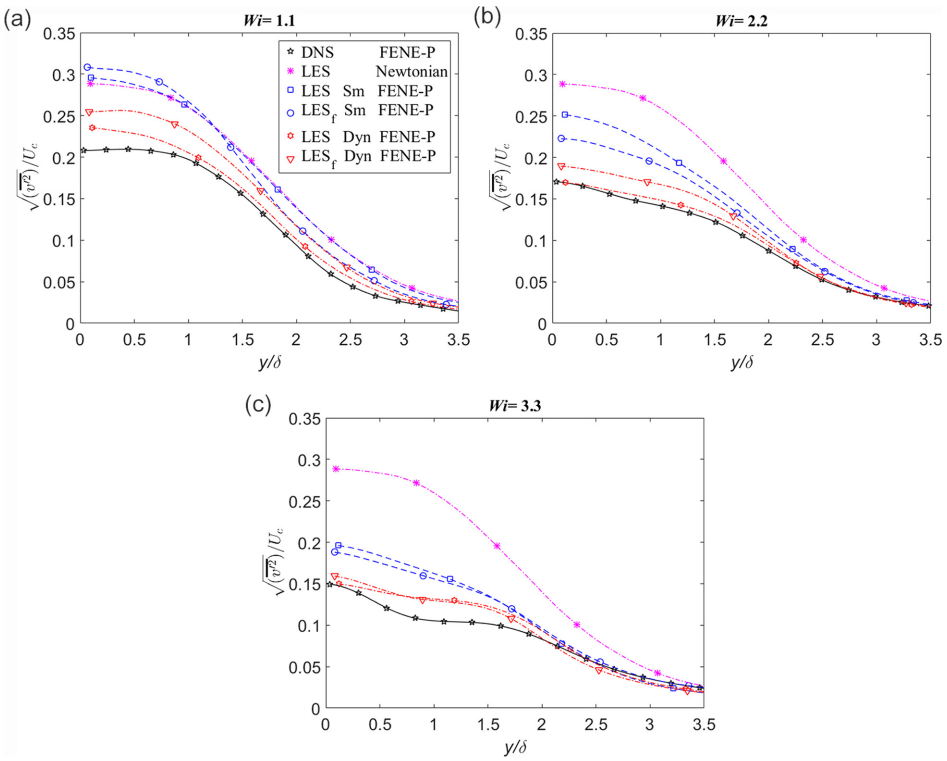

FIG. 21. Effect of SGS stress model on the mean profiles of the rms of the transverse velocity fluctuations $\sqrt{\overline{v'^2}}$, normalized by the centerline mean velocity, at $x/H = 12$ for Wi of (a) 1.1, (b) 2.2, and (c) 3.3. The DSIM closure is used for the SGS polymer stretching in the conformation equation and the Smagorinsky (Sm) and dynamic Smagorinsky (Dyn) for the SGS stress in the momentum equation.

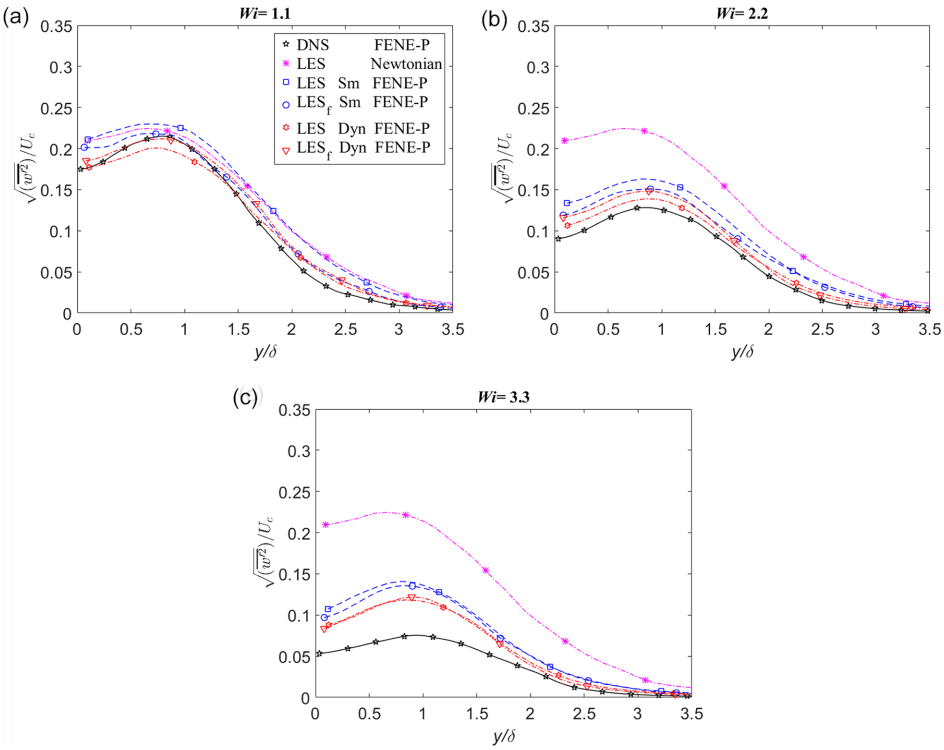

FIG. 22. Effect of SGS stress model on the mean profiles of the rms of the spanwise velocity fluctuations $\sqrt{\overline{w'^2}}$, normalized by the centerline mean velocity, at $x/H = 12$ for Wi of (a) 1.1, (b) 2.2, and (c) 3.3. The DSIM closure is used for the SGS polymer stretching in the conformation equation and the Smagorinsky (Sm) and dynamic Smagorinsky (Dyn) for the SGS stress in the momentum equation.

$$\varepsilon^s = 2\upsilon_s \overline{S'_{ij} S'_{ij}}, \tag{43}$$

and S'_{ij} is the fluctuating rate-of-strain tensor, obtained from

$$S'_{ij} = \frac{1}{2}\left(\frac{\partial u'_i}{\partial x_j} + \frac{\partial u'_j}{\partial x_i}\right). \tag{44}$$

As in Sec. VI B, the overbar denotes averaging in time and in space in the homogeneous direction.

One of the results obtained by Guimarães *et al.*[47] in the development of the theory for viscoelastic planar jets was the identification of the reference velocity and time scales that characterize the flow statistics in the self-similar far field region. In particular, they found that the profiles of polymer stress collapse into the same curve when normalized by $\tau_{p,ref} = \rho U_c^3(x) r^*(d\delta(x)/dx)/(u^*(x)\delta(x))$. They also showed that for sufficiently high Wi numbers these normalized profiles are universal.

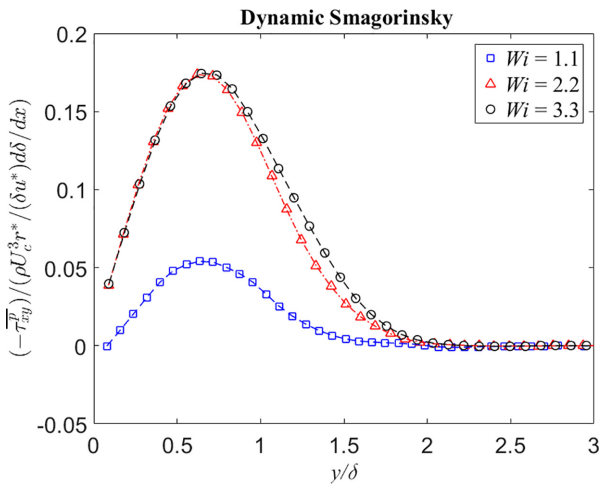

FIG. 23. Mean profiles of polymer shear stress, normalized as in Guimarães *et al.*,[47] for several Weissenberg numbers Wi at $x/H = 12$. SGS stress closed by the dynamic Smagorinsky model.

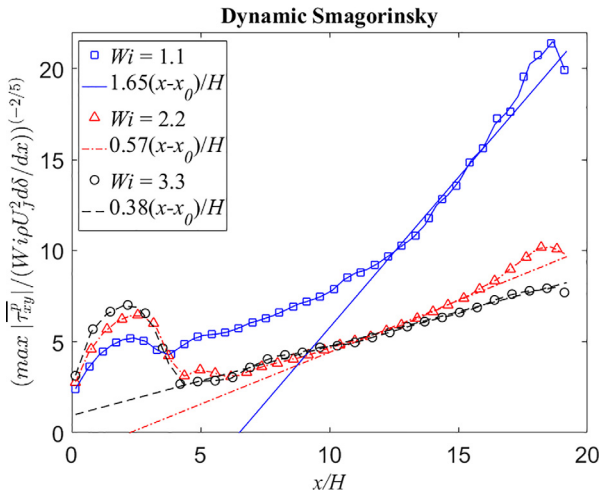

FIG. 24. Streamwise evolution of the maximum value of the mean polymer shear stress, normalized as in Guimarães *et al.*,[47] for several Weissenberg numbers. SGS stress closed by the dynamic Smagorinsky model.

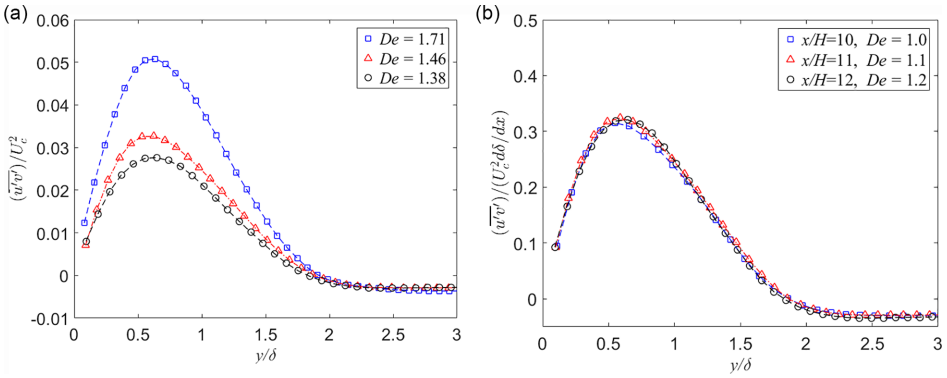

FIG. 25. Transverse profiles of Reynolds shear stress $\overline{u'v'}$ for several *De* numbers normalized by (a) U_c^2 all at $x/H = 12$ and by (b) $U_c^2 d\delta(x)/dx$ at $x/H = 10$, 11, and 12.

Figure 23 shows mean profiles of polymer shear stress normalized by $\tau_{p,ref}$ at $x/H = 12$ for several Weissenberg numbers *Wi*. It is clear that the polymer stresses obtained from the present LES, using the dynamic Smagorinsky and the DSIM closures, collapse at high Weissenberg numbers, in agreement with the theory developed by Guimarães *et al.*[47]

Guimarães *et al.*[47] also derived the scaling of the decay of the maximum polymer stresses, which is described by the following relation:

$$\left(\frac{\tau_c^p(x)}{Wi\rho U_J^2 d\delta(x)/dx}\right)^{-2/5} = A_{\tau_c}\left(\frac{x - x_0}{H}\right), \tag{45}$$

where A_{τ_c} is a scaling factor. Figure 24 shows the streamwise evolution of the normalized maximum polymer shear stresses obtained by LES, with the SGS stresses given by the dynamic Smagorinsky model. It is clear the present results also display the theoretical −5/2 scaling law in the self-similar far-field region, and thus agree with the turbulent viscoelastic jet theory.[47] Moreover, the constant A_{τ_c} decreases with increasing *Wi* numbers displaying values that are consistent with the DNS data of Guimarães *et al.*,[47] particularly for the higher *Wi* numbers, e.g., $Wi \geq 2$ (compare the values of this factor in Tables I and II).

Finally, we assess also the proposed scaling relations for the Reynolds shear stress in viscoelastic turbulent planar jets. Guimarães *et al.*[47] ascertained that the Reynolds shear stress should be normalized as $\overline{u'v'}/(U_c^2 d\delta(x)/dx)$ for similar values of the Deborah number

$$De = \frac{\lambda}{t_c} \tag{46}$$

in order to obtain the corresponding self-similar profiles. In Eq. (46), $t_c = \delta(x)/U_c(x)$ is a convective time scale characteristic of the large energy-carrying eddies.

Figure 25 shows profiles of normalized Reynolds shear stresses for the present LES at a single location ($x/H = 12$) and $Wi = 1.1$, 2.2, and 3.3 [Fig. 25(a)], and at different locations $x/H = 10$, 11, 12, for $Wi = 2.2$ and 3.3 [Fig. 25(b)], but which correspond to approximately the same Deborah numbers ($De \approx 1.0$–1.3). Again, the profiles of the Reynolds stresses normalized as in Guimarães *et al.*[47] collapse into the same profile [Fig. 25(b)], clearly indicating that the present LES recover the expected theoretical profiles observed in the reference DNS.

VII. CONCLUSIONS

In the present work, the DSIM model developed by Ferreira *et al.*[37] for LES of turbulent viscoelastic flows is assessed and tested for the first time in an inhomogeneous turbulent flow configuration. The flow analyzed is a turbulent planar jet, for which a reference DNS exists and a new theory has been recently developed to explain the flow statistics at the far field fully developed turbulent regime (Guimarães *et al.*[47]) The procedure consists in classical *a priori* tests which are based on applying a box filter, with filter sizes $\Delta/\Delta x = 2$, 4, and 8 to separate the resolved and unresolved/subgrid-scale components of the flow, using the reference DNS of viscoelastic turbulent planar jets carried out by Guimarães *et al.*[47]

The analysis revisited all the assumptions previously used by Ferreira *et al.*[37] in isotropic turbulence and considered their validity in turbulent viscoelastic free flows. It turns out that all of these assumptions, and most notably the assumptions of (i) scale similarity of the subgrid-scale polymer stretching terms and (ii) the local equilibrium of the elastic energy production and dissipation, hold remarkably well in the present configuration.

The DSIM model for the SGS polymer stretching term in the constitutive equation, together with the Smagorinsky and dynamic Smagorinsky model for the SGS stress in the momentum equation, was used to carry out LES of the same jets simulated in Guimarães *et al.*[47] although using much coarser grids. The combined dynamic Smagorinsky model and DSIM model gave the best results and demonstrated the ability to predict the flow structures and the classical one point statistics in the flow with reasonable accuracy.

Future work will focus on the extension of the present model for LES of wall-bounded flows.

ACKNOWLEDGMENTS

The authors acknowledge the financial support of Project Nos. PTDC/EMS-ENE/2390/2014 and POCI-01-0145-FEDER-016669 funded by Fundo Europeu de Desenvolvimento Regional, via COMPETE2020-Programa Operacional Competitividade e Internacionalização (POCI) and Fundação para a Ciência e a Tecnologia. In addition, S.P. and F.T.P. also acknowledge financial

support provided by Centro de Estudos de Fenómenos de Transporte through Project Nos. UIDB/00532/2020 and UIDP/00532/2020. C.B.S. is thankful for the support of Fundação para a Ciência e a Tecnologia (FCT), through IDMEC, under LAETA, Project No. UIDB/50022/2020.

DATA AVAILABILITY

The data that support the findings of this study are available from the corresponding author upon reasonable request.

REFERENCES

[1]B. A. Toms, "Some observations on the flow of linear polymer solutions through straight tubes at large Reynolds numbers," in Proceedings of the 1st International Congress on Rheology, North-Holland, Amsterdam (1949), Vol. 2, p. 135.
[2]A. R. Mansour, O. Swaiti, T. Aldoss, and M. Issa, "Drag reduction in turbulent crude oil pipelines using a new chemical solvent," Int. J. Heat Fluid Flow **9**, 316 (1988).
[3]F. C. Li and Y. Kawaguchi, "Investigation on the characteristics of turbulence transport for momentum and heat in a drag-reducing surfactant solution flow," Phys. Fluids **16**, 3281 (2004).
[4]A. G. Fabula, "Fire-fighting benefits of polymeric drag reduction," J. Basic Eng. Trans. ASME **93**(4), 453 (1971).
[5]J. W. Yang, H. Park, H. H. Chun, S. L. Ceccio, M. Perlin, and I. Lee, "Development and performance at high Reynolds number of a skin-friction reducing marine paint using polymer additives," Ocean Eng. **84**, 183 (2014).
[6]T. J. Ober, D. Foresti, and J. A. Lewis, "Active mixing of complex fluids at the microscale," Proc. Natl. Acad. Sci. U. S. A. **112**(40), 12293 (2015).
[7]J. N. Marhefka and M. V. Kameneva, "Natural drag-reducing polymers: Discovery, characterization and potential clinical applications," Fluids **1**, 6 (2016).
[8]A. Pribush, L. Hatzkelzon, D. Meyerstein, and N. Meyerstein, "The mechanism of the polymer-induced drag reduction in blood," Colloids Surf., B **103**, 354 (2013).
[9]W. J. Orts, R. E. Sojka, and G. M. Glenn, "Polymer additives in irrigation water to reduce erosion and better manage water infiltration," Agro-Food-Ind. Hi-Tech **13**, 37(2002).
[10]H. Lee and K. Neville, "The challenge for high polymers in medicine, surgery, and artificial internal organs," J. Macromol. Sci. **4**(3), 757 (1970).
[11]P. C. Sousa, F. T. Pinho, M. S. N. Oliveira, and M. A. Alves, "Extensional flow of blood analog solutions in microfluidic devices," Biomicrofluidics **5**(1), 014108 (2011).
[12]J. L. Lumley, "Drag reduction by additives," Annu. Rev. Fluid Mech. **1**, 367 (1969).
[13]P. S. Virk, "Drag reduction fundamentals," AIChE J. **21**(4), 625 (1975).
[14]C. M. White and M. G. Mungal, "Mechanics and prediction of turbulent drag reduction with polymer additives," Annu. Rev. Fluid Mech. **40**, 235 (2008).
[15]S. B. Pope, *Turbulent Flows* (Cambridge University Press, Cambridge, 2000).
[16]P. Sagaut, *Large Eddy Simulation for Incompressible Flows*, 3rd ed. (Springer, Berlin, 2005).
[17]J. Jiménez, "Computing high-Reynolds-number turbulence: Will simulations ever replace experiments?," J. Turbul. **4**, N22 (2003).
[18]O. Reynolds, "On the dynamical theory of incompressible viscous fluids and the determination of the criterion," Philos. Trans. R. Soc. London, Ser. A **186**, 123–164 (1895), available at http://www.jstor.org/stable/90643.
[19]F. T. Pinho, C. F. Li, B. A. Younis, and R. Sureshkumar, "A low Reynolds number turbulence closure for viscoelastic fluids," J. Non-Newtonian Fluid Mech. **154**, 89 (2008).
[20]F. T. Pinho, C. F. Li, B. A. Younis, and R. Sureshkumar, "Corrigendum to "A low Reynolds number turbulence closure for viscoelastic fluids," J. Non-Newtonian Fluid Mech. **51**, 181 (2012).
[21]P. R. Resende, K. Kim, B. A. Younis, R. Sureshkumar, and F. T. Pinho, "A FENE-P k–ε turbulence model for low and intermediate regimes of polymer-induced drag reduction" J. Non-Newtonian Fluid Mech. **166**, 639 (2011).
[22]G. Iaccarino, E. S. G. Shaqfeh, and Y. Dubief, "Reynolds-averaged modeling of polymer drag reduction in turbulent flows," J. Non-Newtonian Fluid Mech. **165**, 376 (2010).
[23]M. Masoudian, K. Kim, F. T. Pinho, and R. Sureshkumar, "A viscoelastic k-ε-v^2-f turbulent flow model valid up to the maximum drag reduction limit," J. Non-Newtonian Fluid Mech. **202**, 99 (2013).
[24]J. Smagorinsky, "General circulation experiments with the primitive equations," Mon. Weather Rev. **91**(3), 99 (1963).
[25]J. Deardorff, "A numerical study of three-dimensional turbulent channel flow at large Reynolds numbers," J. Fluid Mech. **41**(2), 453 (1970).
[26]M. Lesieur and O. Metais, "New trends in large eddy simulations of turbulence," Annu. Rev. Fluid. Mech. **28**, 45 (1996).
[27]U. Piomelli, "Large-eddy simulation: Achievements and challenges," Prog. Aerosp. Sci. **35**, 335 (1999).
[28]C. Meneveau and J. Katz, "Scale-invariance and turbulence models for large eddy simulation," Annu. Rev. Fluid Mech. **32**, 1 (2000).
[29]C. B. Silva and O. Metais, "On the influence of coherent structures upon interscale interactions in turbulent plane jets," J. Fluid Mech. **473**, 103 (2002).
[30]R. B. Bird, R. C. Armstrong, and O. Hassager, *Dynamics of Polymeric Liquids, Volume 1: Fluid Mechanics* (John Wiley Press, New York, 1987).
[31]R. B. Bird, C. F. Curtiss, R. C. Armstrong, and O. Hassager, *Dynamics of Polymeric Liquids, Volume 2: Kinetic Theory* (John Wiley Press, New York, 1987).
[32]Q. Zhou and R. Akhavan, "A comparison of FENE and FENE-P dumbbell and chain models in turbulent flow," J. Non-Newtonian Fluid Mech. **109**, 115 (2003).
[33]M. Herrchen and H. C. Ottinger, "A detailed comparison of various FENE dumbbell models," J. Non-Newtonian Fluid Mech. **68**, 17 (1997).
[34]R. B. Bird, P. J. Dotson, and N. L. Johnson, "Polymer solution rheology based on a finitely extensible bead-spring chain model," J. Non-Newtonian Fluid Mech. **7**, 213 (1980).
[35]A. Peterlin, "Streaming birefringence of soft linear macromolecules with finite chain length," Polymer **2**, 257 (1961).
[36]Y. Dubief, V. Terrapon, and J. Soria, "On the mechanism of elasto-inertial turbulence," Phys. Fluids **25**, 110817 (2013).
[37]P. O. Ferreira, F. T. Pinho, and C. B. Silva, "Large-eddy simulations of forced isotropic turbulence with viscoelastic fluids described by the FENE-P model," Phys. Fluids **28**, 125104 (2016).
[38]H. D. Xi, E. Bodenschatz, and H. Xu, "Elastic energy flux by flexible polymers in fluid turbulence," Phys. Rev. Lett. **111**, 24501 (2013).
[39]P. C. Valente, C. B. Silva, and F. T. Pinho, "The effect of viscoelasticity on the turbulent kinetic energy cascade," J. Fluid Mech. **760**, 39 (2014).
[40]P. C. Valente, C. B. Silva, and F. T. Pinho, "Energy spectra in inertio-elastic turbulence," Phys. Fluids **28**, 075108 (2016).
[41]T. Watanabe and T. Gotoh, "Hybrid Eulerian-Lagrangian simulations for polymer-turbulence interactions," J. Fluid Mech. **717**, 535 (2013).
[42]T. Ohta and M. Miyashita, "DNS and LES with an extended Smagorinsky model for wall turbulence in non-Newtonian viscous fluids," J. Non-Newtonian Fluid Mech. **206**, 29 (2014).
[43]L. Thais, A. E. Tejada-Martinez, T. B. Gatski, and G. Mompean, "Temporal large eddy simulations of turbulent viscoelastic drag reduction flow," Phys. Fluids **22**, 13103 (2010).
[44]L. Wang, W. H. Cai, and F. C. Li, "Large-eddy simulations of a forced homogenous isotropic turbulence with polymer additives," China Phys. B **23**, 34701 (2014).
[45]J. Li, B. Yu, S. Sun, D. Sun, and Y. Kawaguchi, "An N-parallel FENE-P constitutive model and its application in large-eddy simulation of viscoelastic turbulent drag-reducing flow," J. Comput. Sci. **29**, 70 (2018).
[46]M. Masoudian, C. B. Silva, and F. T. Pinho, "Grid and sub-grid scale interactions in viscoelastic turbulent flow and implications for modelling," J. Turbul. **17**(6), 543 (2016).
[47]M. C. Guimarães, N. Pimentel, F. T. Pinho, and C. B. da Silva, "Direct numerical simulations of turbulent viscoelastic jets," J. Fluid Mech. **899**, A11-1 (2020).
[48]D. Lopes, "Direct and large-eddy simulations of the turbulent entrainment of passive scalars in planar jets," Ph.D. thesis (Instituto Superior Técnico, 2014).

[49]C. B. Silva, D. C. Lopes, and V. Raman, "The effect of subgrid-scale models on the entrainment of a passive scalar in a turbulent planar jet," J. Turbul. **16**(4), 342 (2015).
[50]M. Germano, U. Piomelli, P. Moin, and W. H. Cabot, "A dynamic subgrid-scale eddy viscosity model," Phys. Fluids A **3**, 1760 (1991).
[51]R. Reis, "The dynamics of coherent vortices near the turbulent/non-turbulent interface analysed by direct numerical simulations," Ph.D. thesis (Instituto Superior Técnico, 2011).
[52]S. K. Lele, "Compact finite difference schemes with spectral-like resolution," J. Comp. Phys. **103**, 16 (1992).
[53]S. A. Orszag, "Numerical methods for the simulation of turbulence," Phys. Fluids. **12**(12), II–250 (1969).
[54]F. Dupret and J. M. Marchal, "Loss of evolution in the flow of viscoelastic fluids," J. Non-Newtonian Fluid Mech. **20**, 143–171 (1986).
[55]R. Sureshkumar and A. N. Beris, "Effect of artificial stress diffusivity on the stability of numerical calculations and the flow dynamics of time-dependent viscoelastic flows," J. Non-Newtonian Fluid Mech. **60**, 53 (1995).
[56]T. Min, J. Y. Yoo, and H. Choi, "Effect of spatial discretization schemes on numerical solutions of viscoelastic fluid flows," J. Non-Newtonian Fluid Mech. **100**, 27 (2001).
[57]Y. Dubief and S. K. Lele, *Direct Numerical Simulation of Polymer Flow* (Center for Turbulence Research, Annual Research Briefs, NASA, AMES/Stanford University, 2001), p. 197.
[58]B. Yu and Y. Kawaguchi, "Direct numerical simulation of viscoelastic drag-reducing flow: A faithful finite difference method," J. Non-Newtonian Fluid Mech. **116**, 431 (2004).
[59]T. Vaithianathan and L. R. Collins, "Numerical approach to simulating turbulent flow of a viscoelastic polymer solution," J. Comput. Phys. **187**(1), 1 (2003).
[60]T. Vaithianathan, A. Robert, J. G. Brasseur, and L. R. Collins, "An improved algorithm for simulating three-dimensional, viscoelastic turbulence," J. Non-Newtonian Fluid Mech. **140**(3), 3 (2006).
[61]A. Kurganov and E. Tadmor, "New high-resolution central schemes for nonlinear conservation laws and convection–diffusion equations," J. Comput. Phys. **160**, 241 (2000).
[62]W. Cai, F. Li, and H. Zhang, "DNS study of decaying homogeneous isotropic turbulence with polymer additives," J. Fluid Mech. **665**, 334 (2010).
[63]S. Parvar, C. B. da Silva, and F. T. Pinho, "Local similarity solution for steady laminar planar jet flow of viscoelastic FENE-P fluids," J. Non-Newtonian Fluid Mech. **279**, 104265 (2020).
[64]S. Parvar, C. B. da Silva, and F. T. Pinho, "Corrigendum to "Local similarity solution for steady laminar planar jet flow of viscoelastic FENE-P fluids,"" J. Non-Newtonian Fluid Mech. **279**, 104265 (2020); **281**, 104309 (2020).
[65]S. Liu, C. Meneveau, and J. Katz, "On the properties of similarity subgrid-scale models as deduced from measurements in a turbulent jet," J. Fluid Mech. **275**, 83 (1994).
[66]J. Bardina, J. H. Ferziger, and W. C. Reynolds, Improved subgrid model for large-eddy simulation," AIAA Paper No. 80-1357 (1980).
[67]A. W. Vreman, "An eddy-viscosity subgrid-scale model for the turbulent shear flow: Algebraic theory and applications," Phys. Fluids **16**(10), 3670 (2004).
[68]E. Léveque, F. Toschi, L. Shao, and J.-P. Bertoglio, "Shear-improved Smagorinsky model for large-eddy simulation of wall bounded turbulent flows," J. Fluid Mech. **570**, 491–502 (2007).
[69]R. Sureshkumar, A. N. Beris, and R. A. Handler, "Direct numerical simulation of the turbulent channel flow of a polymer solution," Phys. Fluids **9**, 743 (1997).
[70]K. Kim, C. Li, R. Sureshkumar, S. Balachandar, and R. J. Adrian, "Effects of polymer stresses on eddy structures in drag-reduced turbulent channel flow," J. Fluid Mech. **584**, 281 (2007).
[71]K. Horiuti, K. Matsumoto, and K. Fujiwara, "Remarkable drag reduction in non-affine viscoelastic turbulent flows," Phys. Fluids **25**, 015106 (2013).
[72]M. D. Graham, "Drag reduction and the dynamics of turbulence in simple and complex fluids," Phys. Fluids **26**(10), 101301 (2014).
[73]G. E. Gadd, "Turbulence damping and drag reduction produced by certain additives in water," Nature **206**(4983), 463–467 (1965).
[74]G. E. Gadd, "Reduction of turbulent friction in liquids by dissolved additives," Nature **212**(5065), 874–877 (1966).
[75]A. White, in *Some Observations on the Flow Characteristics of Certain Dilute Macromolecular Solutions, Viscous Drag Reduction*, edited by C. S. Wells (Springer, 1969), pp. 297–311.
[76]A. White, "Turbulence and drag reduction with polymer additives," Ph.D. thesis (Middlesex Polytechnic, 1972).
[77]J. Wu, "Drag reduction in external flows of additive solutions," in *Viscous Drag Reduction*, edited by C. S. Wells (Springer, 1969), pp. 331–350.
[78]E. Gutmark and I. Wygnansky, "The planar turbulent jet," J. Fluid Mech. **73**, 465 (1976).
[79]L. J. S. Browne, R. A. Antonia, S. Rajagopalan, and A. J. Chambers, "Interaction region of a two-dimensional turbulent plane jet in still air," in *Structure of Complex Turbulent Shear Flow, IUTAM Symposium*, edited by R. Dumas and L. Fulachier (Springer, Marseille, 1982).
[80]F. O. Thomas and H. C. Chu, "An experimental investigation of the transition of the planar jet: Subharmonic suppression and upstream feedback," Phys. Fluids **1**(9), 1566 (1989).
[81]R. C. Deo, J. Mi, and G. J. Nathan, "The influence of Reynolds number on a plane jet," Phys. Fluids **20**(7), 075108 (2008).
[82]R. C. Deo, G. J. Nathan, and J. Mi, "Similarity analysis of the momentum field of a subsonic, plane air jet with varying jet-exit and local Reynolds numbers," Phys. Fluids **25**, 015115 (2013).
[83]S. Stanley, A. Sarkar, and J. P. Mellado, "A study of the flowfield evolution and mixing in a planar turbulent jet using direct numerical simulation," J. Fluid Mech. **450**, 377 (2002).
[84]N. S. Berman and H. Tan, "Two-component laser doppler velocimeter studies of submerged jets of dilute polymer solutions," AIChE J. **31**(2), 208 (1985).
[85]K. Koziol and P. Glowacki, "Turbulent jets of dilute polymer solutions," J. Non-Newtonian Fluid Mech. **32**(3), 311 (1989).
[86]A. A. Townsend, *The Structure of Turbulent Shear Flow* (Cambridge University Press, Cambridge, 1976).
[87]J. L. Lumley, "Drag reduction in turbulent flow by polymer additives," J. Polym. Sci. Macromol. Rev. **7**(1), 263 (1973).